Journal Pre-proof

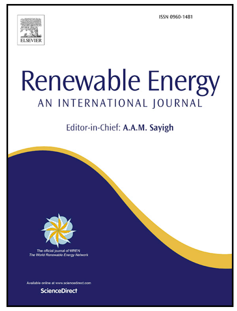

Spectral-splitting hybrid PV-thermal (PVT) systems for combined heat and power provision to dairy farms

Kai Wang, Antonio M. Pantaleo, María Herrando, Michele Faccia, Ioannis Pesmazoglou, Benjamin M. Franchetti, Christos N. Markides

PII: S0960-1481(20)30824-7

DOI: https://doi.org/10.1016/j.renene.2020.05.120

Reference: RENE 13609

To appear in: *Renewable Energy*

Received Date: 9 March 2020

Revised Date: 20 May 2020

Accepted Date: 22 May 2020

Please cite this article as: Wang K, Pantaleo AM, Herrando Marí, Faccia M, Pesmazoglou I, Franchetti BM, Markides CN, Spectral-splitting hybrid PV-thermal (PVT) systems for combined heat and power provision to dairy farms, *Renewable Energy* (2020), doi: https://doi.org/10.1016/j.renene.2020.05.120.

Kai Wang: Conceptualization, Methodology, Software, Validation, Investigation, Writing - Original Draft **Antonio M. Pantaleo:** Data Curation, Writing - Review & Editing **María Herrando:** Writing - Review & Editing **Michele Faccia:** Data Curation **Ioannis Pesmazoglou:** Project administration, Funding acquisition **Benjamin M. Franchetti:** Project administration, Funding acquisition **Christos N. Markides:** Supervision, Resources, Writing - Review & Editing

This is an extended version of a selected paper presented at the 32nd International Conference on Efficiency, Cost, Optimization, Simulation and Environmental Impact of Energy Systems (ECOS2019) held from 23 to 28 June 2019 in Wroclaw, Poland

Spectral-splitting hybrid PV-thermal (PVT) systems for combined heat and power provision to dairy farms

Kai Wang[a,b], Antonio M. Pantaleo[b,c], María Herrando[d], Michele Faccia[e], Ioannis Pesmazoglou[f], Benjamin M. Franchetti[f] and Christos N. Markides[b]*

[a] *Institute of Refrigeration and Cryogenics, Zhejiang University, Hangzhou 310027, China*
[b] *Clean Energy Processes (CEP) Laboratory, Department of Chemical Engineering, Imperial College London, South Kensington Campus, London SW7 2AZ, United Kingdom*
[c] *Department of Agro-Environmental Sciences, University of Bari, Via Amendola 165/A, 70125 Bari, Italy*
[d] *Fluid Mechanics Group, University of Zaragoza, Zaragoza 50007, Spain*
[e] *Department of Soil, Plant and Food Science, University of Bari, via G. Amendola 165/a, 70126 Bari, Italy*
[f] *Solar Flow Ltd., Imperial Innovations, 52 Princes Gate, London SW7 2PG, United Kingdom*
[*]*E-mail: kaiwang19@zju.edu.cn; kai.wang@imperial.ac.uk*

Abstract

Dairy farming is one of the most energy- and emission-intensive industrial sectors, and therefore offers noteworthy opportunities for displacing conventional fossil-fuel consumption both in terms of cost saving and decarbonisation. In this paper, a solar-combined heat and power (S-CHP) system is proposed for dairy farm applications based on spectral-splitting parabolic-trough hybrid photovoltaic-thermal (PVT) collectors, which is capable of providing simultaneous electricity, steam and hot water for processing milk products. A transient numerical model is developed and validated against experimental data to predict the dynamic thermal and electrical characteristics and to assess the thermoeconomic performance of the S-CHP system. A dairy farm in the province of Bari (Italy), with annual thermal and electrical demands of 6,000 MWh and 3,500 MWh respectively, is considered as a case study for considering the energetic and economic potential of the proposed S-CHP system. Hourly simulations are performed over a year using real-time local weather and measured demand-data inputs. The results show that the optical characteristic of the spectrum splitter has a significant influence on the system's thermoeconomic performance. This is therefore optimised to reflect the solar region between 550 nm and 1,000 nm to PV cells for electricity generation and (low-temperature) hot-water production, while directing the rest to solar receivers for (higher-temperature) steam generation. Based on a 10,000-m^2 installed area, it is found that 52% of the demand for steam generation and 40% of the hot water demand can be satisfied by the PVT S-CHP system, along with a net electrical output amounting to 14% of the farm's demand. Economic analyses show that the proposed system is economically viable if the investment cost of the spectrum splitter is lower than 75% of the cost of the parabolic trough concentrator (i.e., <1,950 €/m^2 spectrum splitter) in this application. The influence of utility prices on the system's economics is also analysed and it is found to be significant. An environmental assessment shows that the system has excellent decarbonisation potential (890 tCO_2/year) relative to conventional solutions. Further research efforts should be directed towards the spectrum splitter, and in particular on achieving reductions to the cost of this component, as this leads directly to an increased financial competitiveness of the proposed system.

Keywords:

combined heat and power, dairy, parabolic trough, PV-thermal, PVT, solar energy, spectral splitting

Nomenclature

A	Area, m^2
A'	Ideality factor
b	Empirical parameter
c_e	Electricity price, €/kWh
c_ng	Natural gas price, €/kWh
c	Specific heat capacity, J/(kg·K)
C_0	Total cost, €
$C_\mathrm{O\&M}$	Operation and maintenance costs, €
C_PTC	Cost of parabolic concentrator, €
C_s	Cost saving, €
C_SS	Cost of spectrum splitter, €
d	Discount rate; Density, kg/m^3
D	Diameter, m
e	Charge of an electron, C
E_cov	Covered electricity, €
E_exp	Exported electricity, €
E_g	Bandgap energy, eV
FF	Filling factor
G	Solar irradiance, W/m^2
h	Heat transfer coefficient, W/(m^2·K)
$\hat{h}$	Specific enthalpy, J/kg
i_F	Inflation rate
I	Spectral irradiance, W/(m^2·nm)
J	Current, A
k'	Empirical parameter
k_B	Boltzmann constant
K	Incident angle modifier
$LCOE$	Levelised cost of electricity, €/kWh
m	Empirical parameter
$\dot{m}$	Mass flow rate, kg/s
M	Mass, kg
n	Lifetime, year
N	Day of the year
Nu	Nusselt number
PBT	Payback time, year
Pr	Prandtl number
$\dot{Q}$	Heat flow, W
Q_cov	Thermal energy covered, kWh
Re	Reynolds number
s_e	Electricity exporting price, €/kWh
SR	Spectral response, A/W
t	Time, s
T	Temperature, K
T_st	Solar time, hr
v	Velocity, m/s
V	Voltage, V; Volume, m^3

Greek symbols

α	Absorptivity
β	Temperature coefficient, K^{-1}
δ	Solar declination angle, °
ε	Emissivity
ε_1	Shadowing factor
ε_2	Tracking error
ε_3	Geometry error
ε_4	Dirt effect on mirrors
ε_5	Dirt effect on collector
ε_6	Unaccounted losses
ε_sg	Coefficient for steam generator
ε_wt	Heat transfer effectiveness
θ	Incident angle, °
θ_z	Solar zenith angle, °
ρ_mir	Clean mirror reflectance
η	Efficiency
λ	Wavelength, nm
ρ_ss	Reflectance
σ	Stefan-Boltzmann constant
τ	Transmissivity
φ	Latitude, °
ω	Solar angle, °

Subscripts

a	Ambient
abt	Absorber tube
avg	Average
boil	Boiler

c	Convection	oc	Open circuit
cov	Covered	oil	Oil
dem	Demand	ot	Oil tank
el	Electricity	out	Outlet
exp	Exported	PTC	Parabolic trough concentrator
g	Glass	pv	PV cell
hi	High-temperature	r	Radiation
i	Inner	ref	Reference
in	Inlet	s	Solar radiation
lo	Low-temperature	sc	Short circuit
loss	Thermal loss	sky	Sky
mains	Mains water	th	Thermal
max	Maximum	w	Water
min	Minimum	wc	Water channel
net	Net output	wind	Wind
o	Outer or oil	wt	Water tank

1. Introduction

Dairy farming is one of the most important sectors in the global food industry. The product output of the dairy sector grew by over 15% from 2010 to 2017, including 21% for butter, 16% for cheese, 32% for skim milk powder, and 17% for whole milk powder [1]. In 2017, the world's milk production reached more than 800 million tonnes, 24% of which was produced in the European Union (EU) region. This has placed the EU, together with New Zealand, as the two predominant exporters, both reaching nearly 20 million tonnes per year of equivalent milk. Energy usage on dairy farms has also grown remarkably in the past 20 years due to the increase of number and average size of farms, use of automated equipment, and around-the-clock operation, driven by the increasing demand for dairy products. The Food and Agriculture Organization (FAO) predicts that the total dairy demand will increase by 50% in 2050 compared to the 2010 level [2]. The dairy sector is not only one of the most energy intensive sectors within the food industry but is also considered as one of the most emission intensive sectors. FAO estimated that global greenhouse emissions from the dairy industry accounted for 3% of the total world emissions in 2015 [3]. The implementation of low-carbon efficient technologies and practices would serve as an important pathway to the reduction of dairy emissions.

Processing of milk and milk products requires a considerable amount of electricity and thermal energy. The main energy demands in dairy farms include electricity for pumps, refrigeration, storage, control, separation, lighting, etc., and thermal energy for pasteurisation, evaporation, drying, cleaning, etc. The required temperature of thermal energy ranges from 20 °C to 200 °C, depending on the processes. Typically, low-temperature heat below 80 °C is used for thermisation, pasteurisation, cleaning, preheating, concentration, etc., and higher-temperature heat at around 110 – 180 °C are required for sterilisation, ultra-high temperature processing, drying, etc. Figure 1 shows the typical temperature ranges for different processes in dairy farms [4,5].

Many efforts have been made to facilitate low-emission and energy efficient pathways in the dairy sector. Extensive researches were devoted to assessing energy usage and saving potential in the dairy industry. A study on understanding the energy use in raw milk processing in the UK showed a number of opportunities for energy efficiency improvement, such as low-temperature pasteurisation, alternative homogenisation techniques and reduction in clean-in-place water consumption and temperature [6]. Process optimisation and the use of heat pumps to recover energy from refrigeration units were also suggested. Upton et al. [7] conducted energy audits on three dairy farms at Moorepark (Ireland). Data showed that electricity usage on dairy farms can be reduced by over 50%, through minimisation of hot water leaks, pipe insulations and good management practice for using electricity. Xu et al. [8] analysed the energy usage and performance of global cheese processing industry through literature review, data collection and energy information analyses. The study found that the final energy intensity exhibited significant variations across a few countries and among individual plants, implying large energy saving potential in this sector.

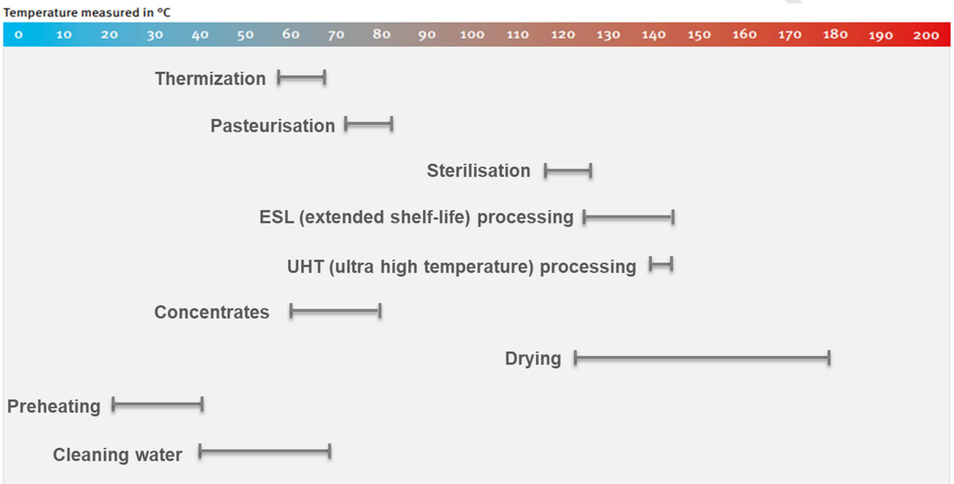

Figure 1. Typical temperature ranges for different processes in dairy farms [4,5].

Solar energy has been widely considered for dairy applications. Cocco et al. [9] investigated the use of a concentrated solar to match the heat and power demands of a typical dairy factory in Italy. The system consisted of linear Fresnel collectors integrated with a two-tank thermal energy storage system, an organic Rankine cycle (ORC) and a solar steam generator. The results demonstrated that the concentrated solar plant could be a promising option for the specified application. Wallerand et al. [10] performed an optimisation of a solar-assisted energy supply system for a dairy farm, which integrated flat plate collectors, photovoltaic (PV) modules, high-concentration PV-thermal (PVT) collectors, and heat pumps into the existing natural gas and grid-electricity based system. The authors demonstrated that the integration of solar technologies, in combination with heat recovery and heat pumping, can reduce the CO_2-equivalent emissions by 65 – 75%. They also concluded that investment in solar energy for such applications can be economically and environmentally attractive for dairy farms if solar energy is optimally integrated and utilised. Sharma et al. [11] assessed the potential of solar heating and the corresponding mitigation of greenhouse gas emissions in the dairy industry in India. This study showed that the solar energy based process heating systems without any storage are estimated to meet 20 – 30% of the total thermal demand of the milk processing in the organised sector of the dairy industry, while mitigating 32 – 144 thousand tonnes of CO_2 emission annually. Atkins et al. [12] performed a thorough pinch analysis of integrating solar thermal energy into low-temperature-pinch dairy processes, taking into account the variable climatic conditions and demand profiles. The study indicated that the appropriate layout of solar heat is vital to the energy saving and it should be integrated above the pinch temperature. Quijera et al. [13] evaluated the viability of integrating a solar thermal system into the conventional energy assets of a dairy plant in Northern Spain. It was concluded that integrating solar energy for the proposed low- and middle-temperature application is technically feasible under the specific climatology by sizing a reasonable solar field, and it can be considered as an energy option for dairy applications. Breen et al. [14] developed a multi-objective optimisation framework for economic and environmental optimisation around equipment, management and electricity tariff choices on dairy farms. The natural-gas based water heating resulted the optimal farm configuration and the alternative solar thermal heating system was not competitive for that application.

According to the literature review, existing solar energy solutions for dairy farms were mainly based on the following three technology routes: standalone PV panels, solar thermal collectors, and side-by-side PV and solar thermal solutions. However, these solutions can only either: i) provide a single type of energy output; ii) have low-efficiency; or iii) need extra installation space for combined heat and power generation. As multi-vector of energy is needed in dairy farms (i.e., electricity, thermal energy at different temperature levels), standalone solar technologies pose limitations on meeting the full-vector energy needs.

Hybrid PVT collectors and systems are an emerging solar combined heat and power (S-CHP) solution, which combines PV and solar thermal technologies, allowing simultaneous electrical and thermal outputs from the same installed area with a much higher overall efficiency than side-by-side standalone PV and solar-thermal systems, if operated appropriately [15,16]. Previous studies have shown that PVT S-CHP systems have promising thermoeconomic potentials in applications where both electricity and low-temperature heat are required, such as residential buildings [17-19], sports centres [20,21], university campuses [22], greenhouses [23], etc. This implies that the hybrid PVT technology may serve as an alternative energy solution for dairy applications.

As the PV module is thermally coupled to the heat transfer fluid and its electrical efficiency drops noticeably with the operating temperature (around −0.4%/°C for silicon solar cells), conventional PVT systems are typically operated below 100 °C, which prevents their application to industrial processes where higher temperature heat is needed [24]. A promising solution to tackle this limitation is to split the incident solar spectrum into two separate bands, one that is directed to PV modules and is well-suited to conversion into electricity, while the rest is absorbed as heat by a thermal absorber [25-27]. This decoupling of the thermal and electrical elements of the collector reduces the PV cell temperatures and allows higher electrical conversion efficiencies, while at the same time supplying heat at temperatures considerably higher than the PV operation temperature.

Studies on spectral-splitting PVT collectors have mainly focused on thermal and optical characterisations of spectrum splitters [28-31], novel concept/prototype developments [32-34], and thermodynamic modelling at the component and system levels [35-37]. The thermal outputs of such PVT systems were explored for either generating additional electricity using power cycles [35,38-39], providing relatively high-temperature heat [40-42], or activating chemical reactions for fuel synthesis [43,44]. Almost all existing modelling work is based on constant temperatures and flow rates predefined for the inlet heat transfer fluid, without any consideration of the coupling between thermal outputs and demands or their transient behaviour under intermittent solar or demand conditions. This can lead to significant under/overestimation of system performance, while also losing insight of its dynamic operation.

More recently, several prototype spectral splitting PVT collectors have been built and different spectrum splitters were investigated. An et al. [45] used the Cu_9S_5 nanofluid as the absorbing filter in a concentrated spectral-splitting PVT collector and the outdoor tests showed that the maximum overall efficiency was 34%, which was 18% higher than that without the filter. Crisostomo et al. [46] conducted outdoor tests of a concentrated spectral-splitting PVT collector with the Ag-SiO_2 nanofluid as the selective absorbing filter for silicon PV cells. The results showed that the spectral-splitting PVT collector delivered 12% more weighted energy output compared with a stand-alone PV system under the same solar irradiance. Otanicar et al. [47] used a gold and indium tin oxide (ITO) nanoparticle-based filter to absorb ultraviolet and visible solar spectrums and achieved thermal and electrical efficiency of 61% and 4% respectively at 110 °C. He et al. [48] explored Ag@TiO2/ethylene glycol/water solution as a nanofluid-based spectral splitter, and obtained an overall efficiency of 84% under 1 kW/m^2 of solar irradiance. Liang et al. experimentally studied spectral splitting PVT collectors based on a SiO_2/TiO_2 interference thin film filter [49] and a glycol-ZnO nanofluid absorbing filter [50], respectively. The results showed that improved overall efficiencies were observed for the spectral splitting PVT collectors compared to those without the filters. These studies demonstrated that spectral splitting PVT collectors and systems with suitable spectral splitters have potential for improved performance and higher operating temperature, which would be attractive for dairy farm applications.

The literature review shows that previous studies on solar energy systems for dairy applications were predominantly focused on standalone PV or solar thermal technologies, or their side-by-side combination, while PVT technologies have rarely been considered. To this end, this work aims to investigate the thermoeconomic performance of a concentrating, spectral-splitting hybrid PVT S-CHP system in dairy farms. Transient simulations are conducted using a whole-system physical model with real-time energy demand and weather data as inputs. Key optical, electrical and heat transfer mechanisms that determine the electrical and thermal performance of the proposed S-CHP are comprehensively considered in the model. The potential of such spectral-splitting PVT systems is then assessed in terms of energetic, economic and environmental metrics.

2. Description of the dairy farm and PVT S-CHP system

A dairy farm located in Province of Bari (Italy) is considered in this study. It has a total area of 16,000 m^2, of which 4,500 m^2 is taken by the dairy production plant. The farm requires two streams of thermal demands, which are supplied by steam and hot water. Steam at 240 °C and 10 bar is used as the heat transfer fluid for processing milk products while hot water is delivered at 70 °C for other low-temperature processes in the farm. A natural-gas-fired steam generator is used in the current energy infrastructure for meeting the thermal demand and the steam is distributed throughout the plant in a closed loop with plate heat exchangers and vapor recovery systems. Grid electricity is used to meet the electrical demand. The farm consumes 681,000 Nm^3 natural gas per year, which is equivalent to about 6,000 MWh heat. The annual electrical demand is about 3,500 MWh. The electricity and natural gas prices for the dairy farm are 0.17 €/kWh and 0.0494 €/kWh (or 0.538 €/Nm^3), respectively. The annual energy bill is around 960 k€.

Quarterly-hour data are available for the total electricity consumption from the dairy farm operator, which is aggregated into hourly electrical demand data over the year, as shown in Figures 2(a) and 2(b). Monthly natural gas demands are also available and are further converted into hourly thermal demand data (see Figures 2(c) and (d)) using the heating value of natural gas, gas boiler efficiency

(82%) and the profile of the electrical demand, assuming that the thermal demand follows the same trend as the electrical demand. The allocation of the high- and low-temperature portions of the thermal demand is assumed as 60% and 40%, respectively.

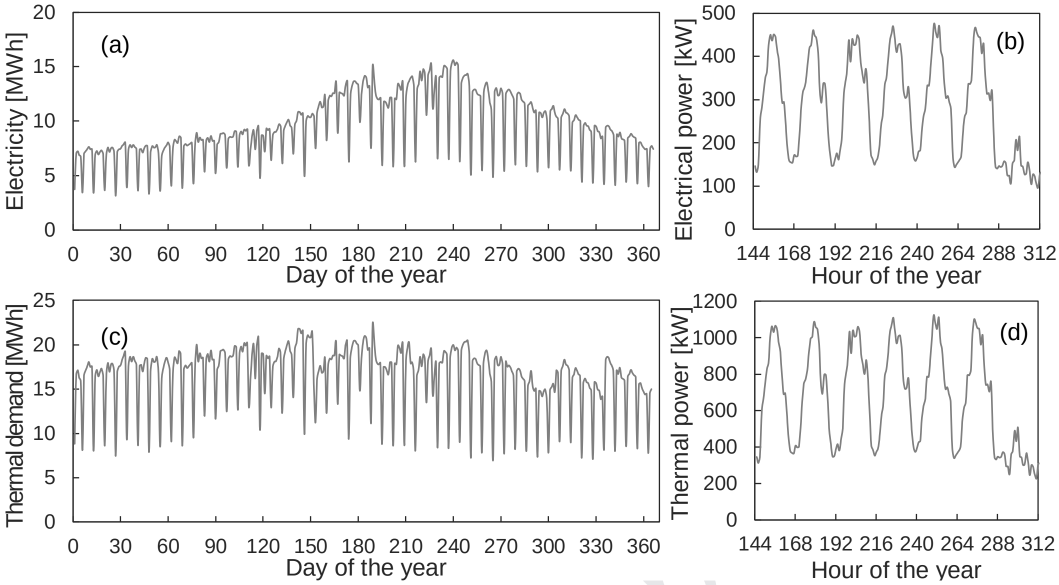

Figure 2. Dairy farm energy demands: (a) hourly electrical demand over a year; (b) hourly electrical power demand on representative days (7th – 13th January); (c) hourly thermal demand over a year; and (d) hourly thermal power demand on representative days (7th – 13th January).

The proposed hybrid S-CHP system for the dairy farm is shown in Figure 3. It comprises parabolic trough concentrated PVT collectors, an oil tank for steam generation (i.e., high-temperature heat), a water tank for hot water provision (i.e., low-temperature heat), inverters and pumps. The PVT collectors use a spectral-splitting design similar to that in Refs. [51,52]. The full solar radiance is reflected and concentrated by the reflective parabolic concentrator. A portion of the concentrated solar radiance, which fits well with the spectrum requirement of the PV cells, is reflected by the spectrum splitters and directed to the cells at the centre of the parabolic trough concentrator, while the rest passes through the splitter and is absorbed by the receivers for generating high-temperature oil. Water flowing in the water channels below the PV cells is used to cool the cells to ensure higher electrical conversion efficiency while generating low-temperature heat for hot water. The detailed structure of the concentrated spectral-splitting PVT collector is illustrated in Figure 3(a).

The spectral characteristics of the spectrum splitter determine how the solar radiance is allocated between the PV cells and the receivers, which further influences the system thermoeconomic performance. Ideally, the filter should be highly reflective in the active spectrum range of PV cells, while highly transparent for the rest of the solar spectrum to generate high-temperature heat through the receivers. In this study, silicon PV cells are used considering their wide deployment and low costs. As shown in Figure 3(b), the electricity generated from the PV modules is used to cover the electricity consumptions of the pumps and the electrical demand, and any surplus is exported to the grid. Electricity is again brought from the grid when the demand exceeds the generation. The selling price of the exported electricity is assumed half of the total purchasing price (i.e., 0.085 €/kWh) since only the generation part of the tariff occurs for the system.

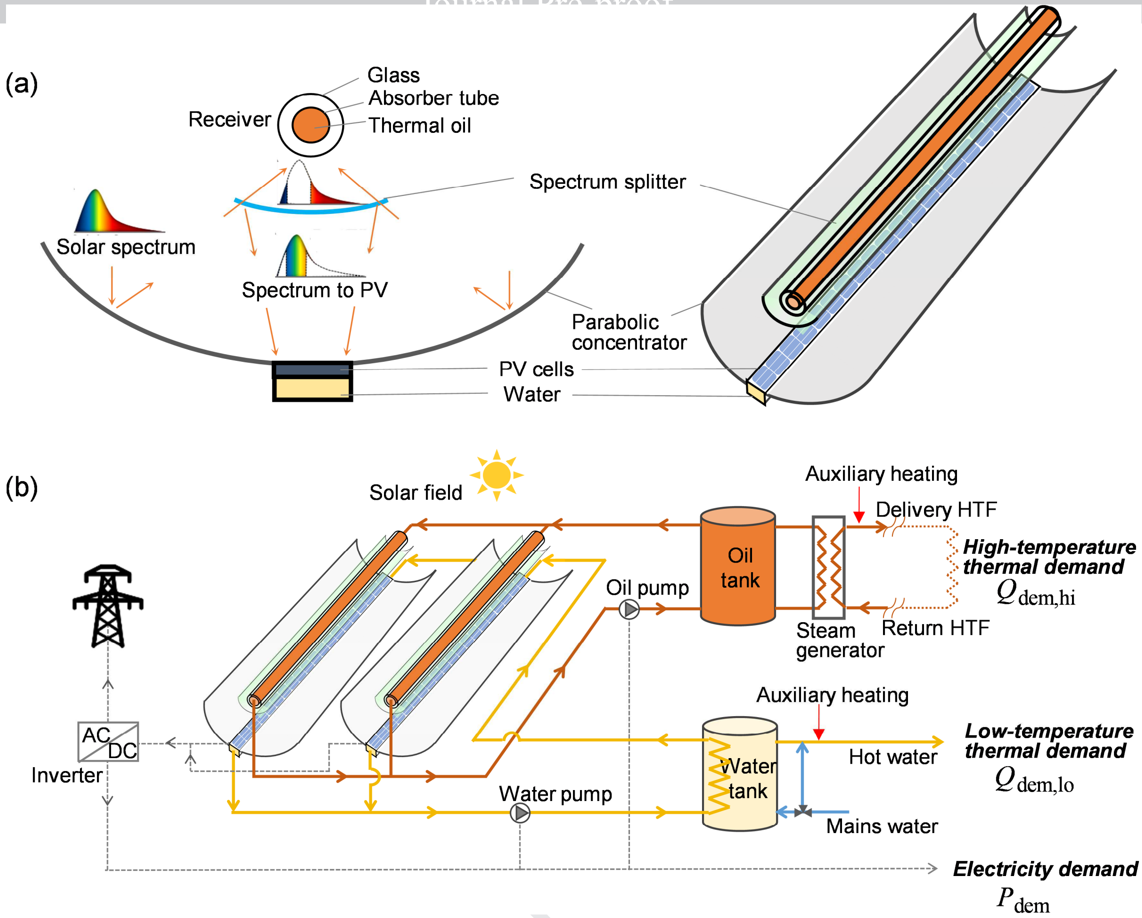

Figure 3. Schematics of the: (a) concentrating, spectral-splitting hybrid PVT collector considered in this work; and (b) proposed whole S-CHP system for dairy applications.

3. Modelling methodology

A transient model has been developed for modelling the proposed spectral-splitting PVT collector and wider S-CHP system, which accounts for the key optical, electrical and heat transfer mechanisms that determine its electrical and thermal performance, while including the synergistic dynamic interactions between the energy generation, storage and demand sides.

3.1. Parabolic trough concentrator

The concentrating spectral-splitting PVT collector is assumed as a modification of the commercial SEGS LS-2 parabolic trough collector [53], by integrating the spectrum splitter and PV modules. The effective optical efficiency of the parabolic trough concentrator is calculated by [53,54],

$$\eta_{\mathrm{PTC}} = \varepsilon_1 \varepsilon_2 \varepsilon_3 \varepsilon_4 \varepsilon_5 \varepsilon_6 \rho_{\mathrm{mir}} K \,, \tag{1}$$

where ε_1 to ε_6 are correction terms accounting for shadowing, tracking and geometry errors, dirt on the mirrors and collectors, and other unaccounted losses, ρ_{mir} is the clean mirror reflectance and K the incident angle modifier (IAM). The values of these terms for calculating the effective optical efficiency of the SEGS LS-2 parabolic trough concentrator are given in Table 1. The IAM is used to correct the optical efficiency when the solar irradiation is not normal to the collector aperture [53],

$$K = \cos(\theta) + 0.000884 \cdot \theta - 0.0000537 \cdot \theta^2 \,, \tag{2}$$

where θ is the incident angle in degrees.

The incident angle, θ, is calculated for East-West tracking with the parabolic trough axis in South-North direction using [55],

$$\cos(\theta) = \sqrt{\cos^2(\theta_z) + \cos^2(\delta) \cdot \cos^2(\omega)}\,. \tag{3}$$

The solar declination angle, δ, for any day of the year, N, can be calculated approximately by,

$$\delta = 23.5 \cdot \sin\left[2\pi \frac{284 + N}{365}\right]. \tag{4}$$

The solar angle, ω, in degrees is calculated using the solar time, T_{st}, in hours,

$$\omega = 15 \cdot (T_{\mathrm{st}} - 12)\,. \tag{5}$$

The solar zenith angle, θ_z, is calculated from,

$$\cos(\theta_z) = \sin(\varphi) \cdot \sin(\delta) + \cos(\varphi) \cdot \cos(\delta) \cdot \cos(\omega)\,, \tag{6}$$

where φ is the latitude in degrees.

Table 1. Correction terms for effective optical efficiency of the parabolic trough concentrator [54].

Parameter	Value
Shadowing factor, ε_1	0.974
Tracking error, ε_2	0.994
Geometry error, ε_3	0.98
Clean mirror reflectance, ρ_{mir}	0.935
Dirt effect on mirrors, ε_4	$0.93/\rho_{\mathrm{mir}}$
Dirt effect on the collector, ε_5	$(1 + \varepsilon_4)/2$
Unaccounted losses, ε_6	0.96

The solar spectrum reaching the ground is dependent on various factors, including the location, air quality, weather conditions, time, season, etc. Air mass 1.5 (AM1.5d) condition is typically used as the reference spectrum distribution in previous studies [35-37,40,51]. However, this method is only a coarse estimation as the actual distribution of the solar spectrum reaching the ground surface varies during a day and over the year, which significantly differs from the ideal AM1.5d distribution. To estimate the time-dependent spectrum distribution, the SPECTRL2 Simple Spectral Model developed by National Renewable Energy Laboratory (NREL) is used [56,57]. An excel tool based on the SPECTRL2 model is used to generate the hourly direct normal spectral solar irradiance given the date, time and location (Bari, 41.1° N, 16.9° E) as the inputs, which are then used as the reference values (I_{ref}) to derive the hourly direct normal spectral solar irradiance based on the solar irradiation data in Bari [57]. To simplify the analysis, the hourly reference solar spectral distributions from the 1st to the 14th days of each month are assumed the same as those in the 1st day of the month, while the reference distributions in the 15th day are used for the rest of that month. The hourly reference solar spectral irradiances in a typical day are given in Figure 4.

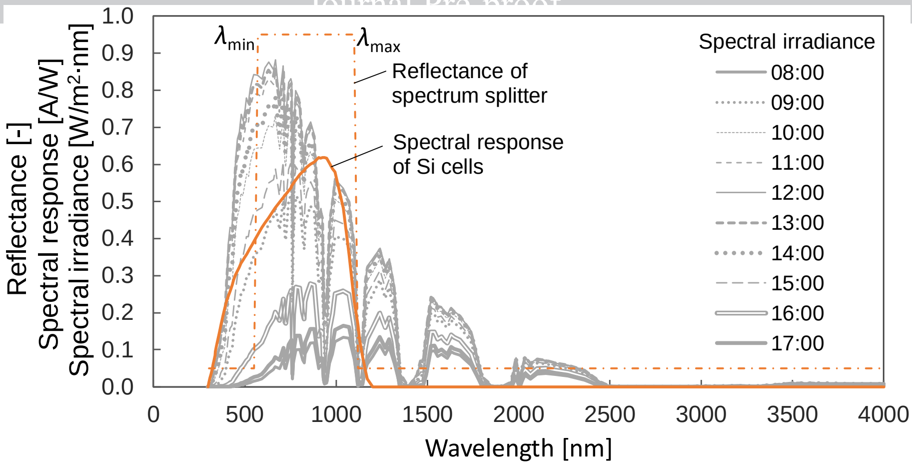

Figure 4. Hourly solar spectral irradiance on the 1st of January, spectral response of Si-cells and reflectance of the spectrum splitter.

3.2. PV cells

3.2.1. Electrical model

Silicon PV cells are considered due to their mass deployment and economic price. Different from the normal operation of PV cells under the whole-spectrum solar irradiance, the PV cells in the proposed S-CHP system are operated under a specific range of the spectrum reflected by the splitters. Two PV electrical efficiencies are defined here: i) the specific electrical efficiency, $\eta_{\mathrm{pv,el1}}$, calculated by dividing the output electricity by the reflected solar energy reaching the PV cells; and ii) the overall electrical efficiency, $\eta_{\mathrm{pv,el2}}$, calculated by dividing the output electricity by the whole-spectrum incident solar energy. These two efficiencies are calculated by [40],

$$\eta_{\mathrm{pv,el1}} = \frac{V_{\mathrm{oc}} \cdot J_{\mathrm{sc}} \cdot FF}{A_{\mathrm{PTC}}\eta_{\mathrm{PTC}} G/G_{\mathrm{ref}} \int_{280}^{4000} \rho_{\mathrm{ss}}(\lambda) I_{\mathrm{ref}}(\lambda)\, \mathrm{d}\lambda} \cdot \left[1 + \beta\left(T_{\mathrm{pv}} - T_{\mathrm{ref}}\right)\right], \tag{7}$$

$$\eta_{\mathrm{pv,el2}} = \frac{V_{\mathrm{oc}} \cdot J_{\mathrm{sc}} \cdot FF}{A_{\mathrm{PTC}} G} \cdot \left[1 + \beta\left(T_{\mathrm{pv}} - T_{\mathrm{ref}}\right)\right], \tag{8}$$

where V_{oc}, J_{sc} and FF are the open-circuit voltage, short-circuit current and filling factor of the PV cells respectively, A_{PTC} is the aperture area of the parabolic trough concentrators, G/G_{ref} is the ratio correcting the actual solar spectral irradiance based on the hourly reference spectral irradiances generated from the SPECTRL2 tool [57], λ is the wavelength, $\rho_{\mathrm{ss}}(\lambda)$ is the spectral reflectance of the spectrum splitters, $I_{\mathrm{ref}}(\lambda)$ is the reference solar spectral irradiance, β is the temperature coefficient of the PV cells, T_{pv} is the PV cell temperature (in °C), and T_{ref} is the reference PV cell temperature (25 °C). The hourly profiles of the reference solar spectral irradiance, $I_{\mathrm{ref}}(\lambda)$, in a typical day (1st January) are given in Figure 4, along with the reflectance, $\rho_{\mathrm{ss}}(\lambda)$, of the spectrum splitters and the spectral responses of the silicon PV cells ($SR(\lambda)$). The total aperture area, A_{PTC}, of the parabolic trough concentrators is set as 10,000 m^2 in this study, which is selected based on the available installation space of the dairy farm. G is the time-dependent local direct normal solar irradiance in Bari, which is given as an input for the model.

The reference solar irradiance, G_{ref}, is calculated by integrating the reference solar spectral irradiance, I_{ref}, reaching the ground at Bari,

$$G_{\mathrm{ref}} = \int_{280}^{4000} I_{\mathrm{ref}}(\lambda)\,\mathrm{d}\lambda\,. \tag{9}$$

The open-circuit voltage, V_{oc}, is calculated by [40,58,59],

$$V_{\mathrm{oc}} = \frac{A' k_{\mathrm{B}} T_{\mathrm{pv}}}{e} \cdot \ln\left(\frac{J_{\mathrm{sc}}}{J_0} + 1\right), \tag{10}$$

where A' is the ideality factor of the PV cells, k_{B} and e denote the Boltzmann constant and the charge of an electron, respectively, J_{sc} and J_0 are the short-circuit current and dark saturation current, respectively. The short-circuit current, J_{sc}, is calculated by [40,58,59],

$$J_{\mathrm{sc}} = A_{\mathrm{PTC}} \eta_{\mathrm{PTC}} G / G_{\mathrm{ref}} \int_{280}^{4000} SR(\lambda) \rho_{\mathrm{ss}}(\lambda) I_{\mathrm{ref}}(\lambda)\,\mathrm{d}\lambda\,, \tag{11}$$

where $SR(\lambda)$ is the spectral response of the PV cells, as given in Figure 4.

The dark saturation current, J_0, is given by,

$$J_0 = k' T_{\mathrm{pv}}^{3/m} \exp\left(\frac{-E_{\mathrm{g}}}{b k_{\mathrm{B}} T_{\mathrm{pv}}}\right), \tag{12}$$

where k', b and m are empirical parameters, and E_{g} is the bandgap energy of the PV cells.

Using the above electrical model, the PV cell efficiency at each time step (1 hour) over a year is calculated based on the local solar irradiance, the reference spectral irradiance and the optical characteristics of the spectrum splitters. A near-ideal spectrum splitter is assumed, and its reflectance is shown in Figure 4. The splitter is highly reflective (ρ_{ss} = 0.95) in the spectrum range that is sensitive to the PV cells, as shown by the range between λ_{min} and λ_{max}. The reflectance of the splitter is near zero (ρ_{ss} = 0.05) and it is almost transparent outside that spectral range in order to allow heat generation from the energy outside the sensitivity range of the PV cells. The absorptivity of the splitter is assumed as zero across the whole spectrum. The DC electricity from the PV cells is first converted to the AC form by the inverters with an assumed efficiency of 0.9, and it is then used to cover the electricity consumption of the pumps and the electrical demand. No battery storage is used in this study, so any surplus electricity is exported to the grid.

3.2.2. Thermal model

The energy balance equation for the PV cells is expressed by,

$$M_{\mathrm{pv}} c_{\mathrm{pv}} \frac{\mathrm{d}T_{\mathrm{pv}}}{\mathrm{d}t} = \dot{Q}_{\mathrm{s,pv}} - \dot{Q}_{\mathrm{r,pv-sky}} - \dot{Q}_{\mathrm{c,pv-a}} - \dot{Q}_{\mathrm{c,pv-w}}\,, \tag{13}$$

where M_{pv} and c_{pv} are the mass and specific heat capacity of the PV cells, respectively. The four terms at the right side of Eq. (13) represent the solar radiation absorbed by the PV cells ($\dot{Q}_{\mathrm{s,pv}}$), radiative heat losses from the PV cells to the sky ($\dot{Q}_{\mathrm{r,pv-sky}}$), convective heat losses from the PV cells to the environment ($\dot{Q}_{\mathrm{c,pv-a}}$), and heat transferred from the PV cells to the heat transfer fluid ($\dot{Q}_{\mathrm{c,pv-w}}$), respectively. The heat transfer fluid for PV cells is water in this case.

The solar radiation absorbed by PV cells, $\dot{Q}_{\mathrm{s,pv}}$, is calculated by integrating the reflectance, $\rho_{\mathrm{ss}}(\lambda)$, of the spectrum splitters with the solar spectral irradiance, $I(\lambda)$, over the solar spectrum,

$$\dot{Q}_{\mathrm{s,pv}} = (\alpha_{\mathrm{pv}} - \eta_{\mathrm{pv}}) A_{\mathrm{PTC}} \eta_{\mathrm{PTC}} G / G_{\mathrm{ref}} \int_{280}^{4000} \rho_{\mathrm{ss}}(\lambda) I_{\mathrm{ref}}(\lambda)\,\mathrm{d}\lambda\,. \tag{14}$$

The radiative losses from the PV cells to the sky, $\dot{Q}_{\mathrm{r,pv-sky}}$, are calculated by,

$$\dot{Q}_{\mathrm{r,pv-sky}} = A_{\mathrm{pv}}\varepsilon_{\mathrm{pv}}\sigma\left(T_{\mathrm{pv}}^{4} - T_{\mathrm{sky}}^{4}\right), \tag{15}$$

where $\varepsilon_{\mathrm{pv}}$ and σ are the emissivity of the PV cells and the Stefan-Boltzmann constant, respectively. The sky temperature, T_{sky}, is estimated in terms of the ambient temperature, T_{a}, using [60],

$$T_{\mathrm{sky}} = 0.0552T_{\mathrm{a}}^{1.5}. \tag{16}$$

The convective heat losses from the PV cells to the ambient are calculated as,

$$\dot{Q}_{\mathrm{c,pv-a}} = A_{\mathrm{pv}}h_{\mathrm{wind}}\left(T_{\mathrm{pv}} - T_{\mathrm{a}}\right), \tag{17}$$

where h_{wind} is the convective heat transfer coefficient accounting for the convection caused by wind passing by the surfaces of PV cells, calculated by [61],

$$h_{\mathrm{wind}} = \begin{Bmatrix} 2.8 + 3v_{\mathrm{wind}} & v_{\mathrm{wind}} \leq 5\ \mathrm{m/s} \\ 6.15v_{\mathrm{wind}}^{0.8} & v_{\mathrm{wind}} > 5\ \mathrm{m/s} \end{Bmatrix}. \tag{18}$$

The last term of Eq. (13), $\dot{Q}_{\mathrm{c,pv-w}}$, is the heat transfer from the PV cells to the heat transfer fluid (i.e., water). The heat transfer mechanisms between the PV cells and the heat transfer fluid include the heat conduction through various layers (glue, Tedlar layer and EVA layer), and the convective heat transfer in the fluid channel. The heat conductance (reverse of resistance) is estimated as 500 W/m^{2}K based on the thickness and thermal conductivity of each layer [62]. The heat transfer from the PV cells to water is then calculated by,

$$\dot{Q}_{\mathrm{c,pv-w}} = A_{\mathrm{pv}}\frac{1}{1/h_{\mathrm{wc}} + 1/500}\left[T_{\mathrm{pv}} - T_{\mathrm{w,avg}}\right], \tag{19}$$

where $T_{\mathrm{w,avg}} = 0.5\left(T_{\mathrm{w,in}} + T_{\mathrm{w,out}}\right)$ is the average water temperature in the water channel under the PV cells, h_{wc} is the convective heat transfer coefficient in the water channel. The water flow is turbulent and thus heat transfer can be calculated using the Dittus-Boelter equation,

$$\mathrm{Nu}_{\mathrm{wc}} = \frac{h_{\mathrm{wc}}D_{\mathrm{wc}}}{k_{\mathrm{w}}} = 0.023\mathrm{Re}^{0.8}\mathrm{Pr}^{0.4}. \tag{20}$$

To simplify the system implementation and considering that the heat from the PV cells is sufficient to meet most of the low-temperature thermal demand for the specified dairy farm application, no thermal insulation is used for the water channel under the PV cells. Therefore, the energy balance of the water in the water channel should account for the heat delivered from the PV cells to the water stream, the convective and radiative heat losses to the surroundings.

$$\dot{m}_{\mathrm{w}}c_{\mathrm{w}}\left(T_{\mathrm{w,out}} - T_{\mathrm{w,in}}\right) = \dot{Q}_{\mathrm{c,pv-w}} - A_{\mathrm{pv}}h_{\mathrm{wind}}\left(T_{\mathrm{w,avg}} - T_{\mathrm{a}}\right) - A_{\mathrm{pv}}\varepsilon_{\mathrm{pv}}\sigma\left(T_{\mathrm{w,avg}}^{4} - T_{\mathrm{a}}^{4}\right), \tag{21}$$

where $\dot{m}_{\mathrm{w}}$ and c_{w} are the mass flow rate and specific heat capacity of the circulating water.

Similar to the electrical efficiencies, the specific thermal efficiency ($\eta_{\mathrm{pv,th1}}$) and the overall thermal efficiency ($\eta_{\mathrm{pv,th2}}$) for the heat collecting element of the PV cells are defined as,

$$\eta_{\mathrm{pv,th1}} = \frac{\dot{m}_{\mathrm{w}}c_{\mathrm{w}}\left(T_{\mathrm{w,out}} - T_{\mathrm{w,in}}\right)}{A_{\mathrm{PTC}}\eta_{\mathrm{PTC}}G/G_{\mathrm{ref}}\int_{280}^{4000}\rho_{\mathrm{ss}}(\lambda)I_{\mathrm{ref}}(\lambda)\,\mathrm{d}\lambda}, \tag{22}$$

$$\eta_{\mathrm{pv,th2}} = \frac{\dot{m}_{\mathrm{w}}c_{\mathrm{w}}\left(T_{\mathrm{w,out}} - T_{\mathrm{w,in}}\right)}{A_{\mathrm{PTC}}G}. \tag{23}$$

The thermal efficiencies defined in Eqs. (22) and (23) are calculated at every time step and thus they are obtained under non-steady states. This is different from the standard tests of solar-thermal collectors where the thermal efficiency is determined when the system reaches the steady state.

3.3. Receiver

The receiver consists of a glass envelope, an absorber tube and thermal oil inside the tube, as in Figure 3(a). The temperature of the glass envelope, T_{g}, is influenced by the convective and radiative losses at the envelope’s outer surface, as well as the radiation between the glass and absorber tube,

$$M_{\mathrm{g}} c_{\mathrm{g}} \frac{\mathrm{d}T_{\mathrm{g}}}{\mathrm{d}t} = \dot{Q}_{\mathrm{s,g}} + \dot{Q}_{\mathrm{r,abt-g}} - \dot{Q}_{\mathrm{r,g-sky}} - \dot{Q}_{\mathrm{c,g-a}} \,, \tag{24}$$

where M_{g} and c_{g} are the mass and specific heat capacity of the glass envelope. The four terms at the right side of Eq. (24) denote the absorbed solar radiation, radiation from the absorber tube to the glass, radiative heat losses to the sky, and convective heat losses to the environment.

It is assumed that the spectrum splitter has zero absorbance and that the regions of the solar spectra that not reflected to the PV cells are all transmitted to the receivers. Therefore, the solar radiation absorbed by the glass, $\dot{Q}_{\mathrm{s,g}}$, is calculated from,

$$\dot{Q}_{\mathrm{s,g}} = \alpha_{\mathrm{g}} A_{\mathrm{PTC}} \eta_{\mathrm{PTC}} G/G_{\mathrm{ref}} \int_{280}^{4000} [1 - \rho_{\mathrm{ss}}(\lambda)] I_{\mathrm{ref}}(\lambda)\, \mathrm{d}\lambda \,, \tag{25}$$

where α_{g} is the average absorptivity of the glass.

The radiative heat transfer from the absorber tube to the glass envelope, $\dot{Q}_{\mathrm{r,abt-g}}$, is obtained by,

$$\dot{Q}_{\mathrm{r,abt-g}} = A_{\mathrm{abt,o}} \sigma \frac{1}{\dfrac{1}{\varepsilon_{\mathrm{abt}}} + \dfrac{1 - \varepsilon_{\mathrm{g}}}{\varepsilon_{\mathrm{g}}} \dfrac{D_{\mathrm{abt,o}}}{D_{\mathrm{g,i}}}} \left(T_{\mathrm{abt}}^4 - T_{\mathrm{g}}^4\right) , \tag{26}$$

where $\varepsilon_{\mathrm{abt}}$ and ε_{g} are the emissivity of the absorber tube and glass, $A_{\mathrm{abt,o}}$ and $D_{\mathrm{abt,o}}$ are the outer surface area and diameter of the absorber tube, T_{abt} and $D_{\mathrm{g,i}}$ denote the absorber tube temperature and the glass inner diameter, respectively.

The radiative heat losses to the sky, $\dot{Q}_{\mathrm{r,g-sky}}$, are calculated using,

$$\dot{Q}_{\mathrm{r,g-sky}} = A_{\mathrm{g,o}} \varepsilon_{\mathrm{g}} \sigma \left(T_{\mathrm{g}}^4 - T_{\mathrm{sky}}^4\right) , \tag{27}$$

where $A_{\mathrm{g,o}}$ is the outer surface area of the glass envelope.

The convective heat losses the environment, $\dot{Q}_{\mathrm{c,g-a}}$, are obtained using,

$$\dot{Q}_{\mathrm{c,g-a}} = A_{\mathrm{g,o}} h_{\mathrm{wind}} \left(T_{\mathrm{g}} - T_{\mathrm{a}}\right) . \tag{28}$$

The energy balance equation for the absorber tube is expressed as,

$$M_{\mathrm{abt}} c_{\mathrm{abt}} \frac{\mathrm{d}T_{\mathrm{abt}}}{\mathrm{d}t} = \dot{Q}_{\mathrm{s,abt}} - \dot{Q}_{\mathrm{r,abt-g}} - \dot{Q}_{\mathrm{c,abt-o}} \,, \tag{29}$$

where M_{abt} and c_{abt} are the mass and specific heat capacity of the absorber tube respectively, and T_{abt} is the absorber tube temperature. The absorbed solar radiation, $\dot{Q}_{\mathrm{s,abt}}$, is calculated by,

$$\dot{Q}_{\mathrm{s,abt}} = \tau_{\mathrm{g}} \alpha_{\mathrm{abt}} A_{\mathrm{PTC}} \eta_{\mathrm{PTC}} G/G_{\mathrm{ref}} \int_{280}^{4000} [1 - \rho_{\mathrm{ss}}(\lambda)] I_{\mathrm{ref}}(\lambda)\, \mathrm{d}\lambda \,, \tag{30}$$

where τ_{g} and α_{abt} are the transmittance of the glass and average absorbance of the absorber tube.

Thermal oil Syltherm-800 is used as the heat transfer fluid, removing absorbed solar heat from the absorber tube. The convective heat transfer from the absorber tube to the thermal oil, $\dot{Q}_{\mathrm{c,abt-o}}$, is,

$$\dot{Q}_{\mathrm{c,abt-o}} = A_{\mathrm{abt,i}} h_{\mathrm{oil}} \left(T_{\mathrm{abt}} - T_{\mathrm{oil,avg}}\right), \tag{31}$$

where $A_{\mathrm{abt,i}}$ is the inner surface area of the absorber tube, and $T_{\mathrm{oil,avg}} = 0.5\left(T_{\mathrm{oil,in}} + T_{\mathrm{oil,out}}\right)$ is the average temperature of the thermal oil in the absorber tube. It should be noted that the thermal oil is circulated between the oil tank and the solar field (see Figure 3(b)). Thus, the oil temperature at the inlet of the absorber tube ($T_{\mathrm{oil,in}}$) equals to the oil tank temperature (T_{ot}). The convective heat transfer coefficient, h_{oil}, is estimated using the Dittus-Boelter equation, similar to Eq. (20).

The energy balance equation for the thermal oil in the absorber tube is expressed as,

$$\dot{m}_{\mathrm{oil}} \left(\hat{h}_{\mathrm{oil,out}} - \hat{h}_{\mathrm{oil,in}}\right) = \dot{Q}_{\mathrm{c,abt-o}}, \tag{32}$$

where $\dot{m}_{\mathrm{oil}}$ is the mass flow rate of the thermal oil through the absorber tube, $\hat{h}_{\mathrm{oil,in}}$ and $\hat{h}_{\mathrm{oil,out}}$ are the specific enthalpy of the oil at the inlet and outlet of the absorber tube, respectively. The specific heat capacity of the thermal oil Syltherm-800 is linearly proportional to the temperature,

$$c_{\mathrm{oil}}(T) = 1.707 \cdot T + 1108\,. \tag{33}$$

The specific enthalpy of the thermal oil Syltherm-800 at a specific temperature is then determined on the basis of the reference state, i.e., 300 K,

$$\hat{h}(T) = \int_{300}^{T} c_{\mathrm{oil}}(T)\mathrm{d}T\,. \tag{34}$$

The specific and overall thermal efficiencies ($\eta_{\mathrm{abt,th1}}$, $\eta_{\mathrm{abt,th2}}$) of the collector are defined as,

$$\eta_{\mathrm{abt,th1}} = \frac{\dot{m}_{\mathrm{oil}} \left(\hat{h}_{\mathrm{oil,out}} - \hat{h}_{\mathrm{oil,in}}\right)}{A_{\mathrm{PTC}} \eta_{\mathrm{PTC}} G / G_{\mathrm{ref}} \int_{280}^{4000} [1 - \rho_{\mathrm{ss}}(\lambda)] I_{\mathrm{ref}}(\lambda)\,\mathrm{d}\lambda}, \tag{35}$$

$$\eta_{\mathrm{abt,th2}} = \frac{\dot{m}_{\mathrm{oil}} \left(\hat{h}_{\mathrm{oil,out}} - \hat{h}_{\mathrm{oil,in}}\right)}{A_{\mathrm{PTC}} G}. \tag{36}$$

3.4. Storage tanks

There are two storage tanks in the proposed S-CHP system, i.e., the water tank and the oil tank for storing low- and high-temperature heat, respectively. To simplify the modelling and also considering the minor influence of stratification to the whole-system performance [16], both the storage tanks are assumed as fully mixed tanks.

3.4.1. Water tank

The thermal energy collected from the PV cells is stored as hot water in the water tank, and it is used for the low-temperature thermal demand. The energy balance equation of the water tank is,

$$M_{\mathrm{wt}} c_{\mathrm{w}} \frac{\mathrm{d}T_{\mathrm{wt}}}{\mathrm{d}t} = \dot{Q}_{\mathrm{w-wt}} - \dot{Q}_{\mathrm{wt,loss}} - \dot{Q}_{\mathrm{cov,lo}}, \tag{37}$$

where M_{wt} and c_{w} are the water mass and specific heat capacity respectively, T_{wt} is the water temperature in the tank, $\dot{Q}_{\mathrm{w-wt}}$ is the heat transferred from water to the water tank through a coil heat exchanger, $\dot{Q}_{\mathrm{wt,loss}}$ is the heat loss to the surroundings and $\dot{Q}_{\mathrm{cov,lo}}$ is the low-temperature thermal demand covered by the water tank.

The heat addition to the water tank, $\dot{Q}_{\mathrm{w-wt}}$, is calculated using the effectiveness-NTU method,

$$\dot{Q}_{\mathrm{w-wt}} = \varepsilon_{\mathrm{wt}} \dot{m}_{\mathrm{w}} c_{\mathrm{w}} \left(T_{\mathrm{w,out}} - T_{\mathrm{wt}}\right), \quad (38)$$

where $\varepsilon_{\mathrm{wt}}$ is the heat transfer effectiveness of the coil heat exchanger inside the tank. When the solar input is too small, the circulating flow is stopped and the heat addition to the tank is zero.

The heat loss of the water tank to the surroundings is calculated by,

$$\dot{Q}_{\mathrm{wt,loss}} = A_{\mathrm{wt}} h_{\mathrm{wt,loss}} (T_{\mathrm{wt}} - T_{\mathrm{a}}), \quad (39)$$

where A_{wt} is the surface area of the water tank and $h_{\mathrm{wt,loss}}$ is the heat loss coefficient.

If the water temperature in the water tank is higher than the required delivery temperature of the low-temperature thermal demand, all of the demand is covered by the tank. If the water temperature in the tank is lower than the required delivery temperature but higher than the mains water temperature, a portion of the demand can be covered while the rest is met by the auxiliary gas boiler. No heat is extracted from the tank if the water temperature is lower than the mains water temperature. Thus, the low-temperature thermal demand covered by the water tank is given by,

$$\dot{Q}_{\mathrm{cov,lo}} = \left\{ \begin{array}{cc} \dot{Q}_{\mathrm{dem,lo}} & T_{\mathrm{wt}} \geq T_{\mathrm{dem,lo}} \\ \dfrac{T_{\mathrm{wt}} - T_{\mathrm{mains}}}{T_{\mathrm{dem,lo}} - T_{\mathrm{mains}}} \dot{Q}_{\mathrm{dem,lo}} & T_{\mathrm{mains}} < T_{\mathrm{wt}} < T_{\mathrm{dem,lo}} \\ 0 & T_{\mathrm{wt}} \leq T_{\mathrm{mains}} \end{array} \right\}, \quad (40)$$

where $\dot{Q}_{\mathrm{dem,lo}}$ is the low-temperature thermal demand of the dairy farm, $T_{\mathrm{dem,lo}}$ is the required delivery temperature of the demand, and T_{mains} is the temperature of mains water.

No thermal losses are assumed for the transfer line between the inlet of the PV cooling channel and the outlet of the coil heat exchanger immersed in the water tank. Therefore, these two temperatures are the same and are calculated by,

$$T_{\mathrm{w,in}} = T_{\mathrm{w,out}} - \varepsilon_{\mathrm{wt}} \left(T_{\mathrm{w,out}} - T_{\mathrm{wt}}\right). \quad (41)$$

3.4.2. Oil tank

The hot thermal oil from the solar field is directly delivered to and stored in the oil tank, while an equivalent amount of oil is extracted from the tank for re-heating in the solar field. The energy balance of the oil tank is expressed as,

$$M_{\mathrm{ot}} \frac{\mathrm{d}\hat{h}_{\mathrm{ot}}}{\mathrm{d}t} = \dot{Q}_{\mathrm{o-ot}} - \dot{Q}_{\mathrm{ot,loss}} - \dot{Q}_{\mathrm{cov,hi}}, \quad (42)$$

where M_{ot} is the total oil mass in the oil tank, $\hat{h}_{\mathrm{ot}}$ is the specific enthalpy of the oil, $\dot{Q}_{\mathrm{o-ot}}$ is the net heat addition to the tank from the hot oil, $\dot{Q}_{\mathrm{ot,loss}}$ is the heat loss to the surroundings, and $\dot{Q}_{\mathrm{cov,hi}}$ is the high-temperature thermal demand covered by the oil tank.

The net heat addition to the oil tank, $\dot{Q}_{\mathrm{o-ot}}$, is calculated by,

$$\dot{Q}_{\mathrm{o-ot}} = \dot{m}_{\mathrm{oil}} \left(\hat{h}_{\mathrm{oil,out}} - \hat{h}_{\mathrm{ot}}\right), \quad (43)$$

where $\hat{h}_{\mathrm{ot}}$ is the specific enthalpy of the oil in the oil tank, calculated using Eq. (34). The circulating oil is stopped and the net heat addition is zero when there is no or too small solar energy input.

The heat loss from the oil tank to the environment is given by,

$$\dot{Q}_{\mathrm{ot,loss}} = A_{\mathrm{ot}} h_{\mathrm{ot,loss}} (T_{\mathrm{ot}} - T_{\mathrm{a}}), \quad (44)$$

where A_{ot} is the surface area of the oil tank and $h_{\mathrm{ot,loss}}$ is the heat loss heat transfer coefficient.

The oil in the oil tank is pumped to a steam generator (see Figure 3(b)) to generate steam, which is required at 240 °C and 10 bar for the investigated dairy farm. The amount of high-temperature heat demand covered by the oil tank depends on the oil temperature in the oil tank and is determined by,

$$\dot{Q}_{\mathrm{cov,hi}} = \begin{cases} \dot{Q}_{\mathrm{dem,hi}} & T_{\mathrm{ot}} \geq \dfrac{T_{\mathrm{dem,hi}} - T_{\mathrm{ret,hi}}}{\varepsilon_{\mathrm{sg}}} + T_{\mathrm{ret,hi}} \\ \dfrac{\varepsilon_{\mathrm{sg}}\left(T_{\mathrm{ot}} - T_{\mathrm{ret,hi}}\right)}{T_{\mathrm{dem,hi}} - T_{\mathrm{ret,hi}}}\dot{Q}_{\mathrm{dem,hi}} & T_{\mathrm{ret,hi}} < T_{\mathrm{ot}} < \dfrac{T_{\mathrm{dem,hi}} - T_{\mathrm{ret,hi}}}{\varepsilon_{\mathrm{sg}}} + T_{\mathrm{ret,hi}} \\ 0 & T_{\mathrm{ot}} \leq T_{\mathrm{ret,hi}} \end{cases}, \tag{45}$$

where $\varepsilon_{\mathrm{sg}}$ is a coefficient to ensure a sufficient temperature difference between the hot oil and water/steam for steam generation, $T_{\mathrm{dem,hi}}$ is the required delivery temperature of the steam (240 °C) and $T_{\mathrm{ret,hi}}$ is the temperature of the returning water (110 °C) in the circulating loop.

3.5. Solving method and model validation

With given initial temperature conditions, hourly weather conditions and demand data, Eqs. (1) to (45) are solved iteratively in MATLAB with a time step of one hour over a whole year. The transient electrical and thermal processes within the system are then obtained, which are further analysed to obtain the energy performance of the whole system, such as the demand covered, annual cost reduction, payback time, etc.

As no experimental data are available for the proposed whole system at the current stage, validation of the model is done separately for the PV cells and parabolic trough collector. Commercial monocrystalline silicon cells (TG18.5BR-BIN34) from bSolar are used in this study [63]. The main electrical parameters of the PV cells under the standard test condition are given in Table 2. The spectral response of the cells is shown in Figure 4. The cells can only be activated by photons with wavelengths between 300 nm and 1,200 nm. The input parameters for the PV electrical model are given in Table 3. As shown in Table 2, the open-circuit voltage, short-circuit current, filling factor and electrical efficiency are all well predicted by the model, with deviations all below 1.5%.

Table 2. Electrical parameters of PV cells and validation of the PV electrical model.

Parameter*	Data from supplier [63]	Data from model	Deviation
Temperature coefficient (β), 1/K	–0.0045		-
Open-circuit voltage (V_{oc}), V	0.612	0.612	0
Short-circuit current (J_{sc}), A	8.75	8.62	1.4%
Filling factor (*FF*)	0.797	0.807	1.3%
Electrical efficiency (η_{pv})	17.5%	17.5%	0%

* These values are valid for the following conditions: light spectrum AM1.5G; light intensity 1,000 W/m^2; measuring temperature 25 °C. The temperature coefficient is a given input value in the model.

Table 3. Model input parameters for the PV electrical model.

Parameter	Value
Empirical parameter, k'	0.06
Empirical parameter, *b*	1.31
Empirical parameter, *m*	0.96

Bandgap energy of silicon cells, E_g	1.1 eV
Ideality factor of PV cells, A'	1.2
Temperature coefficient of PV cells, β	−0.0045/K

The thermal model for the parabolic trough concentrator and receiver is validated on a commercial parabolic trough collector (module: SEGS LS-2) based on the experimental data provided by Sandia National Laboratories [53]. The SEGS LS-2 parabolic trough solar collector was 7.8 m long, with a width of 5 m and an aperture area of 39.2 m^2. The structure of the collector is similar to that in Figure 3(a). The only difference is that the SEGS LS-2 collector does not have a spectrum splitter, thus all the solar irradiance is directed to the receiver. Therefore, the control equations for the SEGS LS-2 collector are the same as Eqs. (24) – (32), only that $\rho_{ss}(\lambda)$ should be zero in this case. Table 4 shows the outlet temperature and collector efficiency data from the tests and simulations. The results show that the deviation for the outlet temperature of the collector is within 0.6% and that for the efficiency is within 4%, with mean values of 0.21% and 1.7% respectively. This indicates that the developed model is valid and has a reliable accuracy, which sets a good basis for further analyses of the proposed concentrated, spectral-splitting PVT system.

Table 4. Validation of the parabolic trough collector model under various conditions on the SEGS LS-2 parabolic trough collector.

No.	G, W/m^2	v_{wind}, m/s	T_a, °C	$\dot{m}_{\mathrm{oil}}$, L/min	$T_{\mathrm{oil,in}}$, °C	$T_{\mathrm{oil,out}}$, °C			η_{PTC}		
						Ref. [53]	Model	Deviation	Ref. [53]	Model	Deviation
1	934	2.6	21.2	47.7	102	124	125	0.5%	73%	75%	2.9%
2	968	3.7	22.4	47.8	151	173	174	0.5%	71%	74%	3.8%
3	982	2.5	24.3	49.1	198	220	220	0.4%	70%	73%	3.5%
4	910	3.3	26.2	54.7	251	269	270	0.1%	70%	71%	0.5%
5	938	1	28.8	55.5	298	317	317	0.1%	68%	68%	0.5%
6	881	2.9	27.5	55.6	299	317	317	-0.1%	69%	68%	-1.8%
7	921	2.6	29.5	56.8	380	398	398	-0.1%	62%	62%	-0.6%
8	903	4.2	31.1	56.3	356	374	374	0%	64%	64%	0.1%
Mean	-	-	-	-	-	-	-	0.2%	-	-	1.7%

Beyond the data in Tables 1 and 3, other parameters used by the model are summarised in Table 5.

Table 5. Main parameters used in the model.

Parameter	Value
Glass envelope [53]	
Outer diameter ($D_{g,o}$), m	0.115
Inner diameter ($D_{g,i}$), m	0.109
Transmittance (τ_g)	0.95
Emissivity (ε_g)	0.86
Absorptivity (α_g)	0.02
Density (d_g), kg/m^3	2,500

Specific heat capacity (c_{g}), J/kg·K	840
Absorber tube [53]	
Outer diameter ($D_{\mathrm{abt,o}}$), m	0.070
Inner diameter ($D_{\mathrm{abt,i}}$), m	0.066
Emissivity ($\varepsilon_{\mathrm{abt}}$)	6.282E-2 + (1.208E-4)T_{abt} + (1.907E-7)T_{abt}^2
Absorptivity (α_{abt})	0.96
Density (d_{abt}), kg/m^3	8,970
Specific heat capacity (c_{abt}), J/kg·K	385
PV cells and accessories	
Emissivity ($\varepsilon_{\mathrm{pv}}$)	0.9
Absorptivity (α_{pv})	0.93
Heat capacity ($M_{\mathrm{pv}}c_{\mathrm{pv}}/A_{\mathrm{pv}}$), J/m^2·K	15,600 [64]
Width (W_{pv}), m	$\pi D_{\mathrm{abt,o}}$
Inverter efficiency	0.9
Oil tank	
Volume (V_{ot}), m^3	$0.01A_{\mathrm{PTC}}$
Diameter (D_{ot}), m	5
Loss coefficient ($h_{\mathrm{ot,loss}}$), W/m^2·K	0.2
Water tank	
Volume (V_{wt}), m^3	$0.01A_{\mathrm{PTC}}$
Diameter (D_{wt}), m	5
Loss coefficient ($h_{\mathrm{wt,loss}}$), W/m^2·K	0.2
Other parameters	
Steam delivery temperature ($T_{\mathrm{dem,hi}}$), °C	240
Return water temperature ($T_{\mathrm{ret,hi}}$), °C	110
Aperture area of solar field (A_{PTC}), m^2	10,000
Heat transfer effectiveness in water tank ($\varepsilon_{\mathrm{wt}}$)	0.4
Coefficient in steam generator ($\varepsilon_{\mathrm{sg}}$)	0.8

3.6. Economic model

Economic analyses are conducted in terms of payback time (*PBT*) and levelised cost of electricity (*LCOE*), considering the system investment cost, operation and maintenance costs, and cost savings due to the reduced natural gas and electricity bills required to satisfy the site's energy demands.

The annual cost saving, C_{s}, is calculated by [20,22],

$$C_{\mathrm{s}} = E_{\mathrm{cov}} \cdot c_{\mathrm{e}} + E_{\mathrm{exp}} \cdot s_{\mathrm{e}} + \frac{Q_{\mathrm{cov}}}{\eta_{\mathrm{boil}}} c_{\mathrm{ng}} - C_{\mathrm{O\&M}}\,, \tag{46}$$

where E_{cov} and Q_{cov} are the electrical and thermal demands covered by the system, E_{exp} the electricity exported to the grid via net metering, c_{e} and c_{ng} the electricity (0.17 €/kWh) and natural gas (0.049 €/kWh) prices, η_{boil} the boiler efficiency (0.82), s_{e} the electricity price for the net metering option applicable to the system (0.085 €/kWh), and $C_{\mathrm{O\&M}}$ the operation and maintenance (O&M) costs. The cost breakdown for the PVT S-CHP system is given in Table 6. As there are no available cost models for the spectrum splitter, its cost is assumed as being within a range of fractions (from 0.05 to 1) of the parabolic trough concentrator, which is a more mature technology.

Table 6. Cost breakdown of the spectral-splitting PVT S-CHP system.

Component	**Cost**	**Ref.**
PV, €/kW	1,000	[65]
Inverter, €/kW	200	[65]
Water tank, €	$0.874 \cdot V_{\mathrm{t}}$ (l)+763.5	[66]
Pump, €	$500 \cdot (P_{\mathrm{pump}}/300)^{0.25}$	[67]
Piping, €	$(0.897+0.21 \cdot D_{\mathrm{pipe}}) \cdot L_{\mathrm{pipe}}$	[67]
Controller, €	500	[67]
Parabolic trough concentrator, €	$170 \cdot A_{\mathrm{PTC}}$	[68]
Oil tank, €	$682 \cdot V_{\mathrm{ot}}$	[69]
Spectrum splitter, €	$(0.05 - 1) \cdot C_{\mathrm{PTC}}$	
Installation cost, €	0.2· total component cost	[67]
Annual O&M cost, €	0.02· total component cost	

The payback time, *PBT*, is calculated from [20,22],

$$PBT = \frac{\ln\left[\frac{C_0(i_{\mathrm{F}} - d)}{C_{\mathrm{s}}} + 1\right]}{\ln\left(\frac{1 + i_{\mathrm{F}}}{1 + d}\right)}, \tag{47}$$

where d is the discount rate (2.8%) and i_{F} the inflation rate (1.2%) assumed for the fuel savings.

The levelised cost of electricity, *LCOE*, is obtained by [20],

$$LCOE = \frac{C_0 + \sum_{i=1}^{n} C_{\mathrm{O\&M}}(1 + i_{\mathrm{F}})^{i-1}(1 + d)^{-i}}{\sum_{i=1}^{n} Q(1 + d)^{-i}}, \tag{48}$$

where Q is the net annual production of energy in the form of electricity. As both thermal energy and electricity are provided from the PVT system, a conversion factor of 0.55 is used from thermal energy to electricity, which corresponds to the typical efficiency of a modern natural gas power plant [20]. The lifetime n is assumed as 25 years. The annual CO_2 emission reduction by the spectral-splitting PVT S-CHP system is also estimated based on the current CO_2 emission factors in Italy (0.206 kgCO_2/kWh for natural gas and 0.350 kgCO_2/kWh for electricity [20]).

4. Results and discussion

Hourly transient simulations were performed in MATLAB over a whole year at the location of Bari (Southern Italy) with input weather data generated using Meteonorm in TRNSYS and site generated demand data. Figure 5 shows the direct solar irradiance, wind speed and ambient temperature.

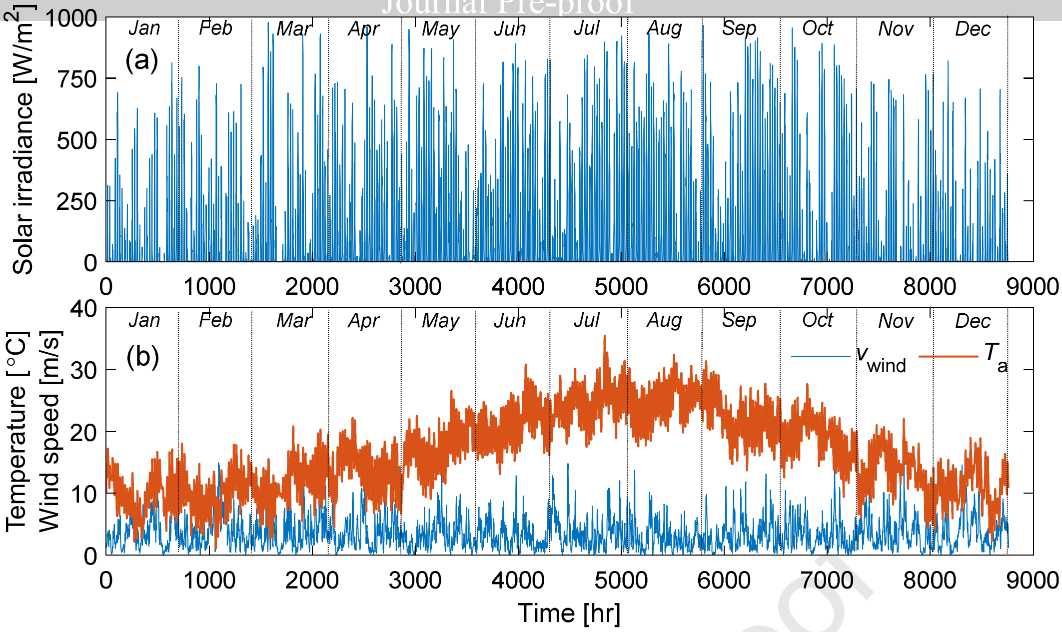

Figure 5. Weather conditions at the considered dairy farm at Bari, Italy: (a) annual solar irradiance (G); and (b) wind speed (v_{wind}) and ambient temperature (T_a).

The optical characteristics of the spectrum splitter determine the allocation of solar radiation between the PV cells and solar thermal absorbers. Thus, the influence of the lower and upper cut-off wavelengths (λ_{min} and λ_{max}) on the payback time of the S-CHP is first investigated. As shown in Figure 6, the cut-off wavelengths significantly influence the payback time. The optimal lower cut-off wavelength is found between 550 nm and 600 nm for each upper cut-off wavelength. The lowest payback time reaches 13.6 years when the lower and upper cut-off wavelengths (λ_{min} and λ_{max}) are respectively 550 nm and 1,000 nm with the cost of the spectrum splitter assumed as 10% of the parabolic trough collector ($0.1 \cdot C_{PTC}$). Here it should be highlighted that the payback time is highly influenced by the electricity and natural gas prices, and thus the above optimal values are valid under the current energy prices in the dairy farm in Bari of Italy.

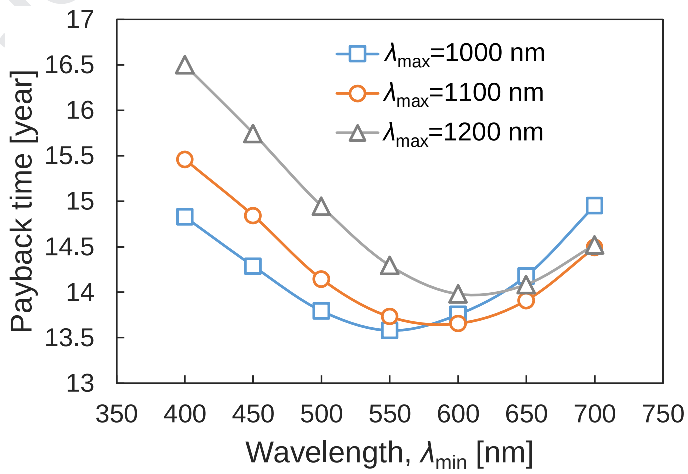

Figure 6. Effect of the two cut-off wavelengths of the spectrum splitter (λ_{min}, λ_{max}) on payback time.

The transient temperature variations of the absorber tube of the receiver, oil tank, PV cells and water tank over the whole year are shown in Figure 7. The overall profiles of the temperatures match with the pattern of the solar irradiance, i.e., high solar irradiance leads to significant increases of the temperatures while low solar irradiance causes noticeable temperature drops. The temperatures are generally higher in summer, due to the lower thermal losses under relatively higher ambient temperatures. It is observed that the temperatures of the PV cells and water tank are mostly below 100 °C, while the oil temperature is normally much higher than 100 °C and reaches up to 400 °C when the solar irradiance is high. The annual average temperatures of water and oil in the tanks are 40 °C and 204 °C, respectively. This implies that the spectral-splitting effectively ensures that the PV cells are operated at low temperatures, which is beneficial for the electricity production and cells' lifetime, while a high-temperature thermal output is also available from the solar receiver which is thermally decoupled from the PV cells.

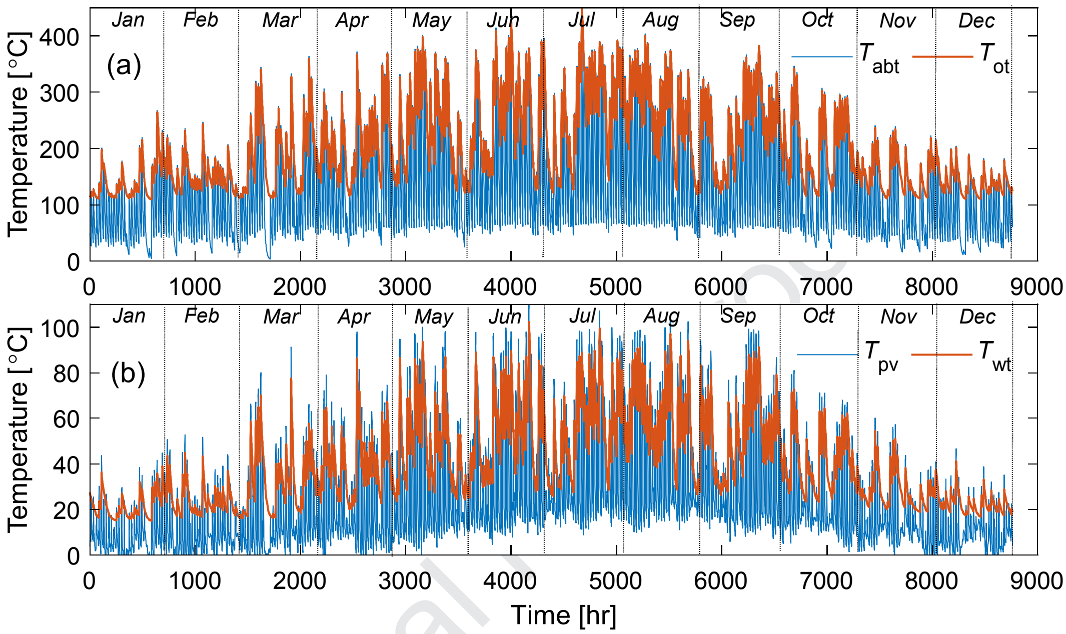

Figure 7. Transient temperatures of the: (a) absorber tube (T_{abt}) and oil tank (T_{ot}) for high-temperature heat; and (b) PV cells (T_{pv}) and water tank (T_{wt}) for low-temperature heat.

The detailed dynamic characteristics of the temperatures for typical seven days in the summer are shown in Figure 8. When there is enough solar irradiance absorbed by the absorber tube and PV cells, their temperatures increase beyond the tank temperatures. The pumps are then triggered, circulating the fluids to deliver the collected thermal energy into the tanks for storage. When the solar irradiance is very low, the temperatures of the absorber tube and PV cells drop below the fluid temperatures in the tanks and thus the pumps are closed in this case.

It can be seen from Figure 8 that the oil tank temperature is between 200 °C and 370 °C and that the water tank temperature is typically between 40 °C and 90 °C. Since the thermal oil is used as both the heat transfer fluid and the storage medium for the high-temperature heat while an intermediate heat transfer loop is used between the PV cells and the water tank, the temperature difference between the absorber tube and the oil tank during the charging processes is lower than that between the PV cells and the water tank, i.e., 4.5 °C *vs*. 8.0 °C on average.

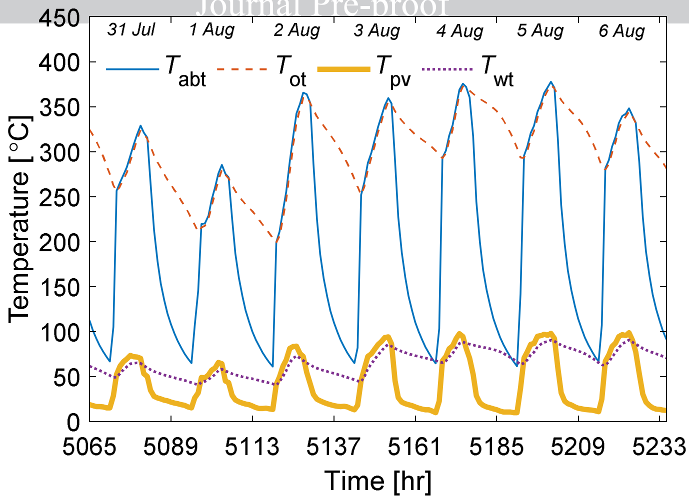

Figure 8. Temperature variations of the absorber tube (T_{abt}), oil tank (T_{ot}), PV cells (T_{pv}) and water tank (T_{wt}) over the period from 31st July to 6th August.

The transient thermal demand profiles and their coverages are shown in Figure 9. During the period of interest, most of the demands can be fully covered, except when the tank temperatures are not sufficiently high to reach the required delivery temperature for the high- and low-temperature thermal demands (240 °C and 70 °C). A natural gas boiler is used as a backup solution, to compensate for the rest of the onsite demand when the solar heating is not enough.

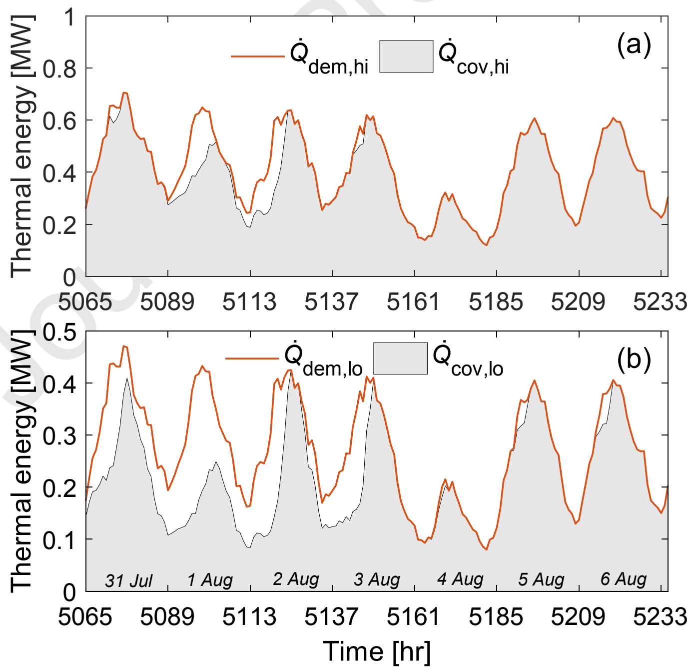

Figure 9. Thermal demand and coverage of the: (a) high-temperature heat ($\dot{Q}_{dem,hi}$ and $\dot{Q}_{cov,hi}$); and (b) low-temperature heat ($\dot{Q}_{dem,lo}$ and $\dot{Q}_{cov,lo}$) demands over the period from 31st July to 6th August.

Figure 10 shows the profiles of the electrical demand, net electricity output and electricity coverage during the period from 31st July to 6th August. The net electricity output is calculated by subtracting the total electricity generated from the PV cells by the electricity consumption of the pumps. The electrical demand is at its peak near the noon time, which coincides with the solar radiation trends and thus the net electricity output profile. It is observed that the electrical demand is always much higher than the net electricity output during the period of interest. Thus, all the net electricity from the S-CHP system is used for covering the electrical demand instantaneously (the grey area as denoted by $\dot{P}_{\text{cov}}$), with no excess exported to the grid. The rest of the electrical demand not fulfilled by the S-CHP system is met by the grid electricity.

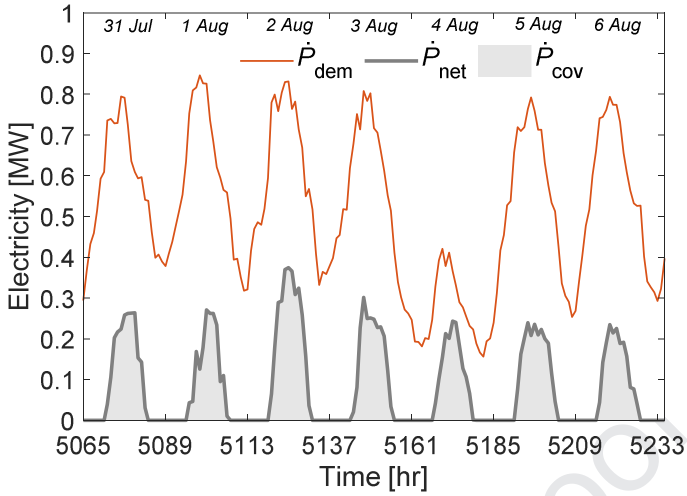

Figure 10. Electrical demand ($\dot{P}_{dem}$), net electricity output ($\dot{P}_{net}$) and instantaneously covered electrical demand ($\dot{P}_{cov}$) over the period from 31^st July to 6^th August.

The specific and overall thermal efficiencies of the heat collection elements of the PV cells ($\eta_{\text{pv,th1}}$ and $\eta_{\text{pv,th2}}$ as defined in Eqs. (22) and (23)) and the parabolic trough collector ($\eta_{\text{abt,th1}}$ and $\eta_{\text{abt,th2}}$ as defined in Eqs. (35) and (36)) are shown in Figure 11. The specific thermal efficiency ($\eta_{\text{pv,th1}}$) of the PV cells, defined by the collected heat from the PV cells divided by the reflected solar energy reaching the PV cells, is around 30 – 50% during the period from 31$^{\text{st}}$ July to 6$^{\text{th}}$ August. As only part of the total solar radiation is reflected to the PV cells, the overall thermal efficiency ($\eta_{\text{pv,th2}}$), calculated by the collected heat from the PV cells divided by the total solar energy, is lower than $\eta_{\text{pv,th1}}$, and it is around 20% at its peak. Similarly, the specific thermal efficiency ($\eta_{\text{abt,th1}}$) of the parabolic trough collector is typically above 55% during the operation period while its overall thermal efficiency ($\eta_{\text{abt,th2}}$) is around 20 – 30%. The peak total thermal efficiency of the S-CHP, defined as the total thermal energy output (i.e., both the low- and high-temperature heat) divided by the total solar energy input, is about 35 – 50% during this period.

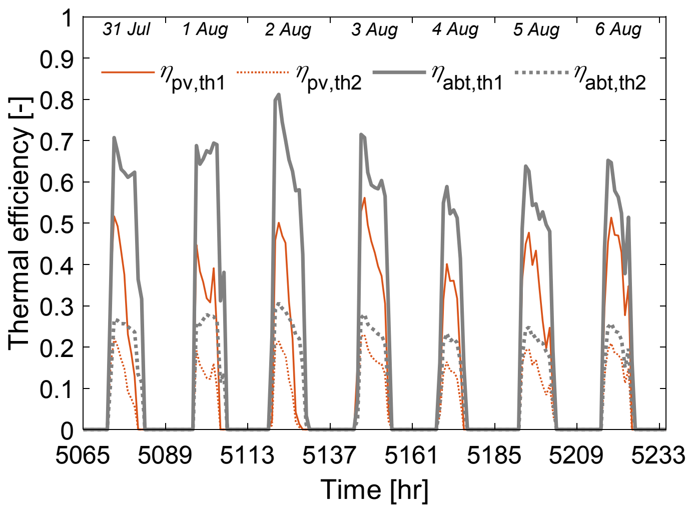

Figure 11. Thermal efficiencies of the PV cell heat collection element ($\eta_{\text{pv,th1}}$, $\eta_{\text{pv,th2}}$) and parabolic trough collector absorber tube ($\eta_{\text{abt,th1}}$, $\eta_{\text{abt,th2}}$) over the period from 31^st July to 6^th August.

Figure 12 shows the tendencies of the specific and overall electrical efficiencies of the PV cells, $\eta_{pv,el1}$ and $\eta_{pv,el2}$, defined as the electricity generated by the PV cells divided by the reflected solar radiation reaching the cells and the total solar radiation respectively (see Eqs. (7) and (8)). As the electrical efficiencies decrease with the operating temperature of the PV cells, $\eta_{pv,el1}$ and $\eta_{pv,el2}$ both decrease from morning to noon, due to the increasing PV cell temperatures, and then increase in the afternoon as the PV cells cool down (see Figure 8). As only part of the incident solar energy is directed to the PV cells, the overall electrical efficiency ($\eta_{pv,el2}$) is only between 5% and 10%, although the specific electrical efficiency ($\eta_{pv,el1}$) of the PV cells is about 15% or above for most of the operational periods.

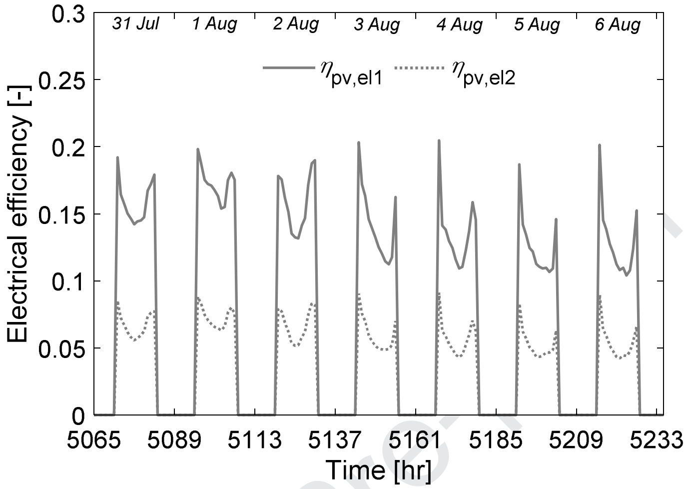

Figure 12. PV cell electrical efficiencies ($\eta_{pv,el1}$, $\eta_{pv,el2}$) over the period from 31st July to 6th August.

Figure 13 shows a summary of the monthly energy demands and coverages. It is found that the proposed spectral-splitting PVT S-CHP system, with an aperture area of 10,000 m^2, is able to cover most of the thermal demands, as shown in Figures 13(a) and (b). The coverage ratio for the thermal demand of steam generation is more than 65% from May to September. Due to the lower solar radiation and higher thermal losses in March, April and October, the coverage ratio is lower but still ranges from 45% to 60%. In the cold months (January, February, November and December), the coverage ratio of the high-temperature heat is around 20 – 30%, with majority of the demands covered by the auxiliary natural gas heating. The thermal energy collected by the receivers covers 52% of the annual high-temperature thermal demands. Similar to the trends of the high-temperature thermal energy, most of the low-temperature thermal demand is covered in the periods from summer to autumn and the annual coverage ratio reaches 40%, as shown in Figure 13(b). The net electricity generation from the PV cells is 14% of the total electrical demand. As the net electricity output is much less than the electrical demand, almost all generated electricity from the S-CHP system is directly used for meeting the demand and thus the amount of the exported electricity is negligible, as shown by the shadows denoted by P_{cov} and P_{exp} in Figure 13(c).

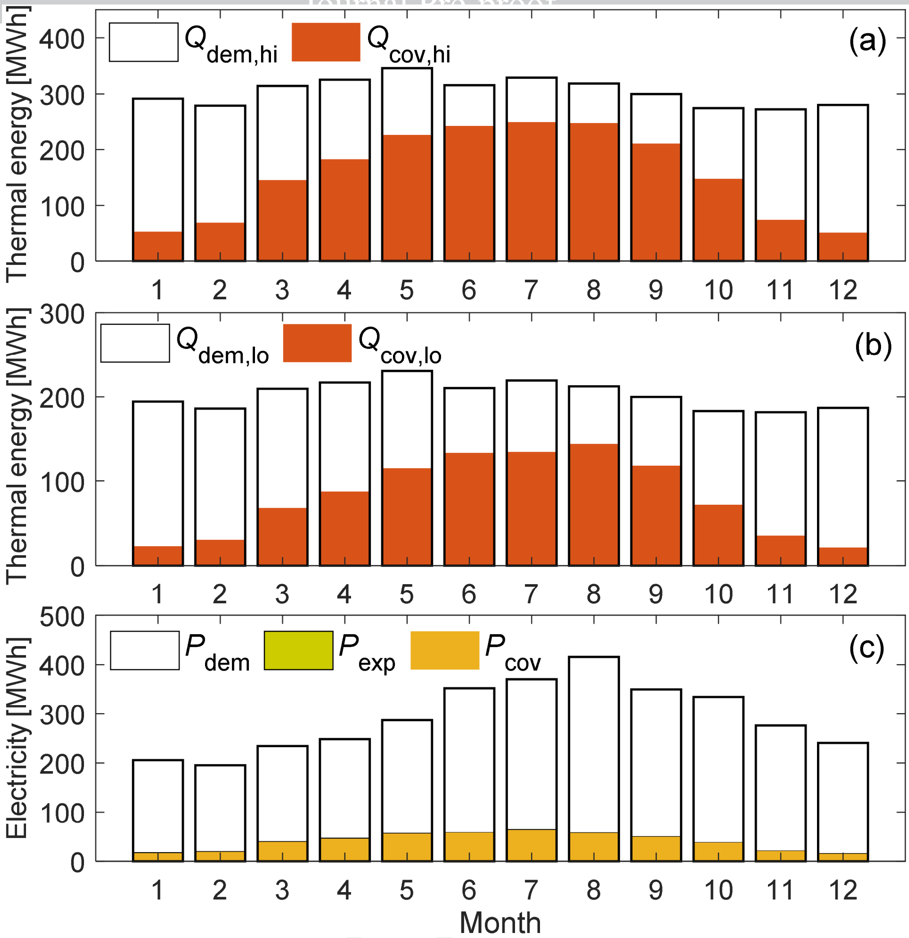

Figure 13. (a) High-temperature thermal demand $Q_{dem,hi}$ and coverage $Q_{cov,hi}$ for steam generation*; (b) low-temperature thermal demand $Q_{dem,lo}$ and coverage $Q_{cov,lo}$ for hot water; and (c) electrical demand P_{dem}, instantaneously covered electricity P_{cov} and exported electricity P_{exp}.*

Based on the energy demand coverages obtained from the thermodynamic modelling, the economic performance of the PVT S-CHP system is further analysed. In particular, since the cost models for spectrum splitters are still not available, the possible range of investment cost of the spectrum splitter (C_{SS}) is estimated based on the total investment cost of the parabolic trough concentrator (C_{PTC}) which is a more established technology with relatively reliable cost estimations, as given in Table 6. Figure 14 shows the sensitivity analyses of the payback time and levelised cost of electricity to the cost of the spectrum splitter. It is found that, for this particular dairy farm application, the investment cost of the spectrum splitter should be less than ~75% of the cost of the parabolic trough concentrator, in order to make the proposed PVT S-CHP system profitable, i.e., *PBT* < 25 years. The payback time ranges from 13 to 25 years when the splitter cost is in the range of 0.05 – 0.75 of the concentrator cost, which corresponds to about 130 – 1,950 € per unit area of the spectrum splitter. The *LCOE* is between 0.089 and 0.141 €/kWh for the splitter costs specified above.

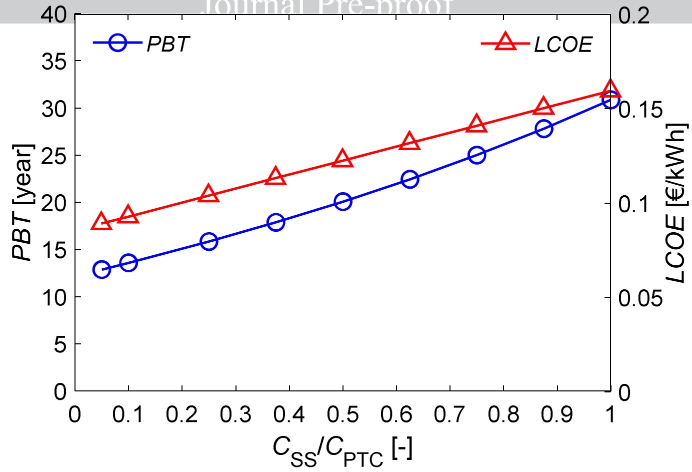

Figure 14. Sensitivity of payback time (PBT) and levelised cost of electricity (LCOE) to the cost of the spectrum splitter (C_{SS}/C_{PTC}).

In order to investigate the influence of energy prices (electricity and natural gas) on the economic performance of the spectral-splitting PVT S-CHP system, three additional price scenarios are also considered: i) the current national utility prices in Italy; ii) the current national utility prices in Denmark, which has high energy prices for natural gas and electricity; and iii) the current national utility prices in Sweden, which has comparable prices between natural gas and electricity [19]. The cut-off wavelengths (λ_{min} and λ_{max}) are optimised for each scenario.

Table 7 shows the thermoeconomic metrics of the spectral-splitting PVT S-CHP system under different energy price scenarios. The results indicate that the cost-competitiveness of the proposed S-CHP is very sensitive to the energy prices. Under the Italian prices which has a slightly higher electricity price and lower natural gas price compared to the current values for the dairy farm, the payback time is increased from 13.6 years to 15.8 years. This is because the amount of the thermal demand is much higher than that of the electricity demand (6,000 MWh/year *vs*. 3,500 MWh/year) and the low natural gas price has stronger influence on the revenue gained from the covered demands. Since the electricity becomes more valuable under this scenario (price ratio c_e/c_{ng} = 4.88, compared to 3.44 under the current price scenario), the spectral range directed to the PV cells is thus widened to increase the electricity generation for a higher revenue, i.e., the optimal upper cut-off wavelength is increased to 1,100 nm. Under the Danish price scenario, the electricity and natural gas prices are both considerably higher, making this S-CHP system a more interesting energy-supply option (*PBT* = 9.1 years). Since the electricity-to-natural gas price ratios are similar between the Danish and current price scenarios (3.50 *vs*. 3.44), the optimal cut-off wavelengths remain the same for both cases. However, under the Swedish energy price scenario, when natural gas is comparably valuable to that of electricity (c_e/c_{ng} = 1.27), the optimal spectral range directed to PV cells narrows to 600 – 1,000 nm, allowing a greater (useful) thermal output. The payback time under Swedish prices is shorter than that under the current local prices for the dairy farm (10.9 years *vs*. 13.6 years), due to the considerably higher price for natural gas.

These results indicate that the proposed S-CHP becomes more cost-competitive if the energy prices increase, which is likely to occur given ongoing increasing energy price trends [19,70]. Further, it is found that in order to make the system more cost-competitive, it is necessary to consider carefully the allocation of the incident solar energy for electrical- *vs*. thermal-energy provision, and that this should be optimised depending on the local electricity-to-natural gas price ratio.

Table 7. Technoeconomic metrics of the spectral-splitting PVT S-CHP system under different energy price scenarios.

Price scenario	Current prices	Italian prices	Danish prices	Swedish prices
Installed area (A_{PTC}), m^2	10,000	10,000	10,000	10,000
Total investment (C_0), M€	2.56	2.56	2.56	2.56
Thermal demand covered for steam generation ($Q_{cov,hi}$), %	52.0	47.3	52.0	60.5
Thermal demand covered for hot water ($Q_{cov,lo}$), %	40.5	43.8	40.5	35.0
Electricity demand covered (P_{cov}), %	13.6	14.3	13.7	12.7
Annual CO_2 emission reduction, tCO_2/year	893	877	893	924
Natural gas price (c_{ng}), €/kWh	0.0494	0.0391	0.0675	0.0727
Electricity price (c_e), €/kWh	0.170	0.191	0.236	0.0922
Price ratio (c_e/c_{ng})	3.44	4.88	3.50	1.27
Optimised cut-off wavelengths ($\lambda_{min} - \lambda_{max}$), nm	550 – 1,000	550 – 1,100	550 – 1,000	600 – 1,000
Payback time (*PBT*) when C_{SS}/C_{PTC} = 0.1, year	13.6	15.8	9.1	10.9

Further incentives for renewable electricity and heating generation, and for high-efficiency cogeneration, are available via the White Certificates mechanism as operated in the Italian energy framework, which provides a contribution around 100 €/TOE (ton oil equivalent) saved. These measures increase the profitability of the investments proposed, but have not been considered in this assessment. The CO_2 emission reduction is estimated at around 890 tons/year, of which the majority, i.e., 80% (720 tons), is associated with the reduced natural gas consumption for heating and the rest with the electricity generation. These findings suggest that the spectral-splitting PVT S-CHP system has an excellent decarbonisation potential relative to conventional solutions, and also that it will be economically viable in the short term in dairy applications if the spectrum splitter can be manufactured at a cost below 1,950 €/m^2. Further research efforts should be directed towards the spectrum splitter [27], and in particular on achieving reductions to the cost of this component, as this leads directly to an increased financial competitiveness of the proposed system.

Being more mature solar technologies, PV-based solar power and PTC-based solar-thermal (ST) systems are both considered as baseline cases. No battery storage is included for the PV-based solar power. The PV model is the same as that in Section 3.2. The PTC-based ST system generates high-temperature heat via thermal oil, which is stored in an oil tank and used for both steam generation and hot water production. The models for the PTCs and the oil tank are similar to those in Section 3. The installation areas of the PV panels and PTCs are the same of the PVT system, i.e., 10,000 m^2. The results are summarised in Table 8. It is found that the PV and ST systems both have slightly shorter payback time compared to the spectral-splitting PVT system for the dairy farm. In particular, due to the lower investment cost, the ST system has the shortest payback time (11.8 years). The electrical demand covered by the PV system is significantly higher than the PVT system (45.3% *vs.* 13.6%), in which a part of solar energy is diverted for thermal energy thus affecting the electricity generation. These results show that for the specified dairy farm application at current energy prices, the PVT system is economically comparable with those more mature alternative solar technologies (in terms of investment and payback time), though slightly less competitive. Nevertheless, its advantage is that it can provide multi-vectors of energy thus enabling more flexibility for its integration with other energy-saving technologies, such as heat pumps, absorption chillers, etc., which may further improve its cost-competitiveness, decarbonisation ability and adaptability to dairy applications.

Table 8. Technoeconomic metrics of the spectral-splitting PVT S-CHP system, PV system, and ST system.

	Spectral-splitting PVT	**PV**	**ST**
Installed area (A_{PTC}), m^2	10,000	10,000	10,000
Total investment (C_0), M€	2.56	2.59	1.88
Thermal demand covered for steam generation ($Q_{cov,hi}$), %	52.0	0	52.6
Thermal demand covered for hot water ($Q_{cov,lo}$), %	40.5	0	92.4
Electricity demand covered (P_{cov}), %	13.6	45.3	0
Annual CO_2 emission reduction, tCO_2/year	893	640	1047
Payback time (*PBT*)	13.6	12.8	11.8

5. Conclusions

A S-CHP system based on hybrid PVT collectors has been studied for the simultaneous provision of combined heat and power to a large dairy farm in Bari, Southern Italy. The system is based on a parabolic trough collector design, but with the addition of a novel spectrum splitter. The purpose of the spectrum splitter is to separate the incident solar spectrum into a spectral band that is suitable for electricity conversion by the silicon PV cells employed in the PVT collector, while the rest is diverted to thermal absorbers for higher-temperature steam generation. The fraction of solar energy that is not converted to electricity by the PV cells is partially recovered by a water loop and provides lower-temperature hot water to the farm, thereby providing simultaneous electricity, steam and hot water, all of which are necessary for processing milk products.

A transient model has been developed, which accounts for the spectrally-selective features of the spectrum splitter, the electrical characteristics of PV cells, and also for the various heat transfer processes through the PVT collector and in wider S-CHP system. The accuracy of the model has been validated based on available experimental data taken from literature.

Annual transient simulations have been performed with hourly weather and demand data used as inputs. The optical characteristics of the spectrum splitter are found to have a significant influence on the thermoeconomic performance of the system, which suggests that these should be optimised for best performance. Given the local energy prices available to the dairy farm under investigation, the optimal wavelength range of the solar spectral region directed to the PV cells is found to be between 550 nm and 1,000 nm. The annual simulation results show that incorporating spectral-splitting technology ensures that the PV cells are operated at relatively low temperatures (40 °C on average) with both electricity and low-temperature heat as outputs, while high-temperature thermal output is simultaneously available from the solar receiver (204 °C on average, allowing easy integration with the existing steam distribution system of the plant).

Based on an installed area of 10,000 m^2, the annual thermal energy produced by the PVT S-CHP system has been shown to cover a little over half (52%) of the high-temperature thermal demand for steam generation and around 40% of the low-temperature thermal demand for hot water by the dairy farm. The net electricity generation of the S-CHP system amounts to 14% of the total electrical demand, and almost all of the generated electricity is used instantaneously onsite for covering the farm's demand, with a negligible amount of excess electricity exported to the grid.

Complementary economic analyses have shown that, in order to make the proposed system profitable within its lifetime, the investment cost of the spectrum splitter should be less than about 75% of the cost of the parabolic concentrator in the proposed application, i.e., 1,950 €/m^2, or lower. The payback time ranges from 13 to 25 years when the splitter cost is between 0.05 and 0.75 of the concentrator cost, corresponding to between 130 and 1,950 €/m^2 for the spectrum splitter. In order to understand the influence of utility prices on the economic performance of the spectral-splitting PVT S-CHP system, three scenarios with current national utility prices of three countries have been assessed: i) Italy, where the study is based; ii) Denmark, which is selected as it has favourable energy prices; and iii) Sweden, where electricity and natural gas have similar price levels. The results show that the cost-competitiveness of the S-CHP system is very sensitive to the energy prices, and it becomes economically interesting if the energy prices reach Danish levels, which is likely to occur given the continuing trends of increasing energy prices. With the current energy costs for the dairy farm, the CO_2 emission reduction is estimated to be 890 tons/year, of which 720 tons originate from the reduced consumption of natural gas and the rest from displaced electricity.

This work suggests that such concentrating spectral-splitting PVT S-CHP systems have an excellent decarbonisation potential, and further efforts should be directed towards proposing spectrum-splitter designs with a cost that would make the system economically viable.

Acknowledgments

This is an extended version of a selected paper presented at the 32nd International Conference on Efficiency, Cost, Optimization, Simulation and Environmental Impact of Energy Systems (ECOS2019) held from 23 to 28 June 2019 in Wroclaw, Poland. This work was supported by the UK Engineering and Physical Sciences Research Council (EPSRC) [grant number EP/M025012/1]. The authors would also like to thank UK company Solar Flow (www.solar-flow.co.uk). Data supporting this publication can be obtained on request from cep-lab@imperial.ac.uk.

References

[1] The world dairy situation 2018, Bulletin of the International Dairy Federation No. 494/2018. International Dairy Federation, Brussels, Belgium, 2018.

[2] World livestock 2011: Livestock in food security. Food and Agriculture Organization of the United Nations, Rome, Italy, 2011.

[3] Climate change and the global dairy cattle sector: The role of the dairy sector in a low-carbon future. Food and Agriculture Organization of the United Nations and Global Dairy Platform Inc., Rome, Italy, 2019.

[4] Deeth HC, Lewis MJ. High temperature processing of milk and milk products. John Wiley & Sons Ltd., West Sussex, UK, 2017.

[5] Ramos A, Guarracino I, Mellor A, Alonso-Álvarez D, Childs P, Ekins-Daukes NJ, et al. Solar-thermal and hybrid photovoltaic-thermal systems for renewable heating. Briefing paper No 22, Grantham Institute Imperial College London; May 2017. p. 1–9. [https://www.imperial.ac.uk/media/imperial-college/grantham-institute/public/publications/briefing-papers/2679_Briefing-P-22-Solar-heat_web.pdf]
[6] Industrial energy efficiency accelerator: Guide to the dairy sector (CTG033). Carbon Trust, London, UK, 2010.
[7] Upton J, Murphy M, French P, Dillon P. Dairy farm energy consumption. Teagasc National Dairy Conference 2010:87-97. 2010.
[8] Xu T, Flapper J, Kramer KJ. Characterization of energy use and performance of global cheese processing. Energy 34:1993-2000, 2009.
[9] Cocco D, Tola V, Petrollese M. Application of concentrating solar technologies in the dairy sector for the combined production of heat and power. Energy Proc 101:1159-66, 2016.
[10] Wallerand AS, Kermani M, Voillat R, Kantor I, Maréchal F. Optimal design of solar-assisted industrial processes considering heat pumping: Case study of a dairy. Renew Energy 128:565-85, 2018.
[11] Sharma AK, Sharma C, Mullick SC, Kandpal TC. Potential of solar industrial process heating in dairy industry in India and consequent carbon mitigation. J Clean Prod 140:714-24, 2017.
[12] Atkins MJ, Walmsley MRW, Morrison AS. Integration of solar thermal for improved energy efficiency in low-temperature-pinch industrial processes. Energy 35:1867-73, 2010.
[13] Quijera JA, Alriols MG, Labidi J. Integration of a solar thermal system in a dairy process. Renew Energy 36:1843-53, 2011.
[14] Breen M, Murphy MD, Upton J. Development of a dairy multi-objective optimization (DAIRYMOO) method for economic and environmental optimization of dairy farms. Appl Energy 242:1697-711, 2019.
[15] Mellor A, Alonso Alvarez D, Guarracino I, Ramos A, Riverola Lacasta A, Ferre Llin L, et al. Roadmap for the next-generation of hybrid photovoltaic-thermal solar energy collectors. Sol Energy 174:386-98, 2018.
[16] Guarracino I, Mellor A, Ekins-Daukes NJ, Markides CN. Dynamic coupled thermal-and-electrical modelling of sheet-and-tube hybrid photovoltaic/thermal (PVT) collectors. Appl Therm Eng 101:778-95, 2016.
[17] Herrando M, Markides CN. Hybrid PV and solar-thermal systems for domestic heat and power provision in the UK: Techno-economic considerations. Appl Energy 161:512-32, 2016.
[18] Ramos A, Chatzopoulou MA, Guarracino I, Freeman J, Markides CN. Hybrid photovoltaic-thermal solar systems for combined heating, cooling and power provision in the urban environment. Energy Convers Manage 150:838-50, 2017.
[19] Herrando M, Ramos A, Zabalza I. Cost competitiveness of a novel PVT-based solar combined heating and power system: Influence of economic parameters and financial incentives. Energy Convers Manage 166:758-70, 2018.
[20] Wang K, Herrando M, Pantaleo AM, Markides CN. Technoeconomic assessments of hybrid photovoltaic-thermal vs. conventional solar-energy systems: Case studies in heat and power provision to sports centres. Appl Energy 254:113657, 2019.
[21] Wang K, Herrando M, Pantaleo AM, Markides CN. Thermoeconomic assessment of a PV/T combined heating and power system for University Sport Centre of Bari. Energy Proc 158:1229-34, 2019.
[22] Herrando M, Pantaleo AM, Wang K, Markides CN. Solar combined cooling, heating and power systems based on hybrid PVT, PV or solar-thermal collectors for building applications. Renew Energy 143:637-47, 2019.

[23] Wang K, Pantaleo AM, Mugnozza GS, Markides CN. Technoeconomic assessment of solar combined heat and power systems based on hybrid PVT collectors in greenhouse applications. IOP Conf Ser Mater Sci Eng 609:72026, 2019.

[24] Kalogirou S. The potential of solar industrial process heat applications. Appl Energy 76:337-61, 2003.

[25] Joshi SS, Dhoble AS. Photovoltaic-thermal systems (PVT): Technology review and future trends. Renew Sustain Energy Rev 92:848-82, 2018.

[26] Mojiri A, Taylor R, Thomsen E, Rosengarten G. Spectral beam splitting for efficient conversion of solar energy–a review. Renew Sustain Energy Rev 28:654-63, 2013.

[27] Huang G, Riera Curt S, Wang K, Markides CN. Challenges and opportunities for nanomaterials in spectral splitting for high-performance hybrid solar photovoltaic-thermal applications: a review. Nano Mater Sci, 2020 [in press], https://doi.org/10.1016/j.nanoms.2020.03.008.

[28] Looser R, Vivar M, Everett V. Spectral characterisation and long-term performance analysis of various commercial heat transfer fluids (HTF) as direct-absorption filters for CPV-T beam-splitting applications. Appl Energy 113:1496-511, 2014.

[29] Vivar M, Everett V. A review of optical and thermal transfer fluids used for optical adaptation or beam-splitting in concentrating solar systems. Prog Photovolt Res Appl 22:612-33, 2014.

[30] Crisostomo F, Taylor RA, Zhang T, Perez-Wurfl I, Rosengarten G, Everett V, et al. Experimental testing of SiN_x/SiO_2 thin film filters for a concentrating solar hybrid PV/T collector. Renew Energy 72:79-87, 2014.

[31] Adam SA, Ju X, Zhang Z, Lin J, Abd El-Samie MM, Xu C. Effect of temperature on the stability and optical properties of SiO2-water nanofluids for hybrid photovoltaic/thermal applications. Appl Therm Eng 175:115394, 2020.

[32] Mojiri A, Stanley C, Taylor RA, Kalantar-zadeh K, Rosengarten G. A spectrally splitting photovoltaic-thermal hybrid receiver utilising direct absorption and wave interference light filtering. Sol Energy Mater Sol Cell 139:71-80, 2015.

[33] Widyolar B, Jiang L, Abdelhamid M, Winston R. Design and modeling of a spectrum-splitting hybrid CSP-CPV parabolic trough using two-stage high concentration optics and dual junction InGaP/GaAs solar cells. Sol Energy 165:75-84, 2018.

[34] Hangweirer M, Höller R, Schneider H. Design and analysis of a novel concentrated photovoltaic-thermal receiver concept. Jpn J Appl Phys 54(8S1):08KE01, 2015.

[35] Liu Y, Hu P, Zhang Q, Chen Z. Thermodynamic and optical analysis for a CPV/T hybrid system with beam splitter and fully tracked linear Fresnel reflector concentrator utilizing sloped panels. Sol Energy 103:191-9, 2014.

[36] Brekke N, Dale J, DeJarnette D, Hari P, Orosz M, Roberts K, et al. Detailed performance model of a hybrid photovoltaic/thermal system utilizing selective spectral nanofluid absorption. Renew Energy 123:683-93, 2018.

[37] Crisostomo F, Taylor RA, Surjadi D, Mojiri A, Rosengarten G, Hawkes ER. Spectral splitting strategy and optical model for the development of a concentrating hybrid PV/T collector. Appl Energy 141:238-46, 2015.

[38] Branz HM, Regan W, Gerst KJ, Borak JB, Santori EA. Hybrid solar converters for maximum exergy and inexpensive dispatchable electricity. Energy Environ Sci 8(11):3083-91, 2015.

[39] Bierman DM, Lenert A, Wang EN. Spectral splitting optimization for high-efficiency solar photovoltaic and thermal power generation. Appl Phys Lett 109:243904, 2016.

[40] Ni J, Li J, An W, Zhu T. Performance analysis of nanofluid-based spectral splitting PV/T system in combined heating and power application. Appl Therm Eng 129:1160-70, 2018.

[41] Zhao J, Song Y, Lam W, Liu W, Liu Y, Zhang Y, et al. Solar radiation transfer and performance analysis of an optimum photovoltaic/thermal system. Energy Convers Manage 52:1343-53, 2011.
[42] Rodrigues Fernandes M, Schaefer LA. Long-term environmental impacts of a small-scale spectral filtering concentrated photovoltaic-thermal system. Energy Convers Manage 184:350-61, 2019.
[43] Hogerwaard J, Dincer I, Naterer GF. Experimental investigation and optimization of integrated photovoltaic and photoelectrochemical hydrogen generation. Energy Convers Manage 207: 112541, 2020.
[44] Ling Y, Li W, Jin J, Yu Y, Hao Y, Jin H. A spectral-splitting photovoltaic-thermochemical system for energy storage and solar power generation. Appl Energy 260:113631, 2020.
[45] An W, Wu J, Zhu T, Zhu Q. Experimental investigation of a concentrating PV/T collector with Cu_9S_5 nanofluid spectral splitting filter. Appl Energy 184:197-206, 2016.
[46] Crisostomo F, Hjerrild N, Mesgari S, Li Q, Taylor RA. A hybrid PV/T collector using spectrally selective absorbing nanofluids. Appl Energy 193:1-14, 2017.
[47] Otanicar T, Dale J, Orosz M, Brekke N, DeJarnette D, Tunkara E, et al. Experimental evaluation of a prototype hybrid CPV/T system utilizing a nanoparticle fluid absorber at elevated temperatures. Appl Energy 228:1531-39, 2018
[48] He Y, Hu Y, Li H. An Ag@TiO_2/ethylene glycol/water solution as a nanofluid-based beam splitter for photovoltaic/thermal applications in cold regions. Energy Convers Manage 198:111838, 2019.
[49] Liang H, Han H, Wang F, Cheng Z, Lin B, Pan Y, et al. Experimental investigation on spectral splitting of photovoltaic/thermal hybrid system with two-axis sun tracking based on SiO_2/TiO_2 interference thin film. Energy Convers Manage 188:230-40, 2019.
[50] Liang H, Wang F, Zhang D, Cheng Z, Zhang C, Lin B, et al. Experimental investigation of cost-effective ZnO nanofluid based spectral splitting CPV/T system. Energy 194:116913, 2020.
[51] Widyolar B, Jiang L, Winston R. Spectral beam splitting in hybrid PV/T parabolic trough systems for power generation. Appl Energy 209:236-50, 2018.
[52] Jiang S, Hu P, Mo S, Chen Z. Optical modeling for a two-stage parabolic trough concentrating photovoltaic/thermal system using spectral beam splitting technology. Sol Energy Mater Sol Cell 94:1686-96, 2010.
[53] Dudley VE, Kolb GJ, Mahoney AR, Mancini TR, Matthews CW, Sloan M, et al. Test results: SEGS LS-2 solar collector. Sandia National Laboratories, Albuquerque, USA, 1994.
[54] Forristall R. Heat transfer analysis and modeling of a parabolic trough solar receiver implemented in engineering equation solver. National Renewable Energy Laboratory, Golden, USA, 2003.
[55] Bellos E, Tzivanidis C, Belessiotis V. Daily performance of parabolic trough solar collectors. Sol Energy 158:663-78, 2017.
[56] Bird RE, Riordan C. Simple solar spectral model for direct and diffuse irradiance on horizontal and tilted planes at the earth's surface for cloudless atmospheres. J Climate Appl Meteor 25:87-97, 1986.
[57] https://www.nrel.gov/grid/solar-resource/spectral.html [accessed 28/01/2020].
[58] Otanicar T, Chowdhury I, Phelan PE, Prasher R. Parametric analysis of a coupled photovoltaic/thermal concentrating solar collector for electricity generation. J Appl Phys 108:114907, 2010.
[59] Otanicar TP, Chowdhury I, Prasher R, Phelan PE. Band-gap tuned direct absorption for a hybrid concentrating solar photovoltaic/thermal system. J Sol Energy Eng 133(4):041014, 2011.
[60] Notton G, Cristofari C, Mattei M, Poggi P. Modelling of a double-glass photovoltaic module using finite differences. Appl Therm Eng 25:2854-77, 2005.
[61] Sharples S, Charlesworth PS. Full-scale measurements of wind-induced convective heat transfer from a roof-mounted flat plate solar collector. Sol Energy 62:69-77, 1998.

[62] Herrando M, Markides CN, Hellgardt K. A UK-based assessment of hybrid PV and solar-thermal systems for domestic heating and power: system performance. Appl Energy 122:288-309, 2014.

[63] http://www.b-solar.com/Pictures/Monofacial%20TG18.5BR_D200.pdf [accessed 22/01/2020].

[64] Guarracino I. Hybrid photovoltaic and solar thermal (PVT) systems for solar combined heat and power. Imperial College London, London, UK, 2017.

[65] Petrollese M, Cocco D. Optimal design of a hybrid CSP-PV plant for achieving the full dispatchability of solar energy power plants. Sol Energy 137:477-89, 2016.

[66] Herrando M, Ramos A, Freeman J, Zabalza I, Markides CN. Technoeconomic modelling and optimisation of solar combined heat and power systems based on flat-box PVT collectors for domestic applications. Energy Convers Manage 175:67-85, 2018.

[67] Quoilin S, Declaye S, Tchanche BF, Lemort V. Thermo-economic optimization of waste heat recovery organic Rankine cycles. Appl Therm Eng 31:2885-93, 2011.

[68] Kurup P, Turchi CS. Parabolic trough collector cost update for the System Advisor Model (SAM), Technical Report NREL/TP-6A20-65228. National Renewable Energy Laboratory, Golden, USA, 2015.

[69] Aguilar-Jiménez JA, Velázquez N, Acuña A, Cota R, González E, González L, et al. Techno-economic analysis of a hybrid PV-CSP system with thermal energy storage applied to isolated microgrids. Sol Energy 174:55-65, 2018.

[70] https://ec.europa.eu/eurostat/data/database [accessed 28/01/2020].

Highlights

- Spectral-splitting parabolic-trough PVT based CHP system proposed for dairy farms.
- Simultaneous electricity, steam and hot water can be provided.
- Dynamic thermal and electrical characteristics of the PVT system are analysed.
- 550-1,000 nm to PV for electricity & hot water and the rest to receivers for steam.
- Economically viable if spectrum splitter cost is < 75% of parabolic trough cost.

Declaration of interests

☒ The authors declare that they have no known competing financial interests or personal relationships that could have appeared to influence the work reported in this paper.

☐The authors declare the following financial interests/personal relationships which may be considered as potential competing interests: